The Chick Optic Tectum Developmental Stages. A Dynamic Table Based on Temporal- and Spatial-Dependent Histogenetic Changes: A Structural, Morphometric and Immunocytochemical Analysis

Melina Rapacioli,[1] Alejandra Rodríguez Celín,[1] Santiago Duarte,[2] Ana Laura Ortalli,[2] Jennifer Di Napoli,[2] Luisa Teruel,[2] Viviana Sánchez,[2] Gabriel Scicolone,[2] and Vladimir Flores[1,2]*

[1]*Department of Biostructural Sciences, Interdisciplinary Group in Theoretical Biology, Favaloro University, Argentina*
[2]*Laboratory of Developmental Neurobiology, Institute of Cell Biology and Neurosciences "Prof. E. De Robertis," School of Medicine, University of Buenos Aires, Argentina*

ABSTRACT Development is often described as temporal sequences of developmental stages (DSs). When tables of DS are defined exclusively in the time domain they cannot discriminate histogenetic differences between different positions along a spatial reference axis. We introduce a table of DSs for the developing chick optic tectum (OT) based on time- and space-dependent changes in quantitative morphometric parameters, qualitative histogenetic features and immunocytochemical pattern of several developmentally active molecules (Notch1, Hes5, NeuroD1, β-III-Tubulin, synaptotagmin-I and neurofilament-M). Seven DSs and four transitional stages were defined from ED2 to ED12, when the basic OT cortical organization is established, along a spatial developmental gradient axis extending between a zone of maximal and a zone of minimal development. The table of DSs reveals that DSs do not only progress as a function of time but also display a spatially organized propagation along the developmental gradient axis. The complex and dynamic character of the OT development is documented by the fact that several DSs are simultaneously present at any ED or any embryonic stage. The table of DSs allows interpreting how developmental cell behaviors are temporally and spatially organized and explains how different DSs appear as a function of both time and space. The table of DSs provides a reference system to characterize the OT corticogenesis and to reliably compare observations made in different specimens. J. Morphol. 000:000–000, 2011.

KEY WORDS: developmental stages; developmental axis; corticogenesis; cell proliferation; spatio-temporal organisation

INTRODUCTION

Development is commonly described as sequences of quasi-discrete developmental stages (DSs), i.e., tables of developmental stages (Streeter, 1948; Hamburger and Hamilton, 1951; Eyal-Giladi and Kochav, 1976; O'Rahilly and Muller, 1987; Hopwood, 2007). Tables of DSs for the whole embryo are usually based on morphogenetic changes while tables of DSs for particular organs are based on histogenetic changes, developmental cell behavior, and the expression pattern of signaling proteins, receptors, and transcription factors. As an example, three basic DSs were described in the developing optic tectum (OT) by analyzing the neuroepithelial (NE) cells proliferation (Fujita, 1967, 1997; Mey and Thanos, 2000; Fujita, 2003). The developmental expression of microtubule associated proteins (Matus, 1990; Johnson and Jope, 1992) was later used to re-interpret the OT development (Yasuda and Fujita, 2003) and allows the description of four DSs that appropriately correlate with those described earlier by Fujita (1964, 1967, 1997).

This study aims at presenting a table of DSs for the developing OT based on qualitative features and quantitative data, as well as on the spatio-temporal expression pattern of several proteins which regulate cell behavior in the developing CNS [Notch1, Hes5, NeuroD1, β-III Tubulin (βIIITub), synaptotagmin I (Syt) and middle-molecular weight neurofilament (NF-M)]. Notch signaling is involved in proliferation, differentiation and

Additional Supporting Information may be found in the online version of this article.

Contract grant sponsor: CONICET (Argentina); Contract grant number: PIP6003; Contract grant sponsor: University of Buenos Aires; Contract grant number: UBACYT M029.

*Correspondence to: Vladimir Flores, Favaloro University, Solís 453 (1078), Buenos Aires, Argentina.
E-mail: vflores@favaloro.edu.ar

Received 16 March 2010; Revised 26 November 2010; Accepted 5 December 2010

Published online in Wiley Online Library (wileyonlinelibrary.com)
DOI: 10.1002/jmor.10943

neuritogenesis (Giniger, 1998; Irvin et al., 2001; Whitford et al., 2002; Lai, 2004; Basak and Taylor, 2007; Cisneros et al., 2008). NeuroD1 participates in neuron determination and differentiation (Katayama et al., 1997; Morrow et al., 1999; Cho and Tsai, 2004; Sanes et al., 2006). βIIITub is involved in neuronal differentiation and axonogenesis (Moody et al., 1989; Lee et al., 1990; Jiang and Oblinger, 1992; Haendel et al., 1996; Molea et al., 1999). The neuron-specific protein NF-M is involved in neuritogenesis (Striedter and Beydler, 1997; Lalonde and Strazielle, 2003; Yasuda and Fujita, 2003; Perrot et al., 2008). Synaptotagmin, a synaptic vesicle-specific protein, participates in neuritogenesis and synaptogenesis (Littleton et al., 1993, 1995; Lou and Bixby, 1993; Kabayama et al., 1999).

Tables of DSs are usually based on temporal changes and disregard differences between tissues located at different positions along a spatial axis. The developing OT exhibits significant differences in mitotic NE cell density (Rapacioli et al., 2000; Mazzeo et al., 2004) and postmitotic neuronal migration (Rapacioli et al., 2001a, 2001b, 2005) along the cephalic-caudal (cph-cd) axis. It has been proposed that this spatial asymmetry could be due to temporal differences in the onset and ending of both cell behaviors as a function of the space. If this proposal were correct, DSs should exhibit a spatially organized propagation along the cph-cd axis: (a) ordered sequences of areas, corresponding to increasing DSs, should be found along the cd-cph axis at any embryonic day (ED) and, reciprocally, (b) the area corresponding to each DS should change its position along the cph-cd axis as a function of the ED.

MATERIALS AND METHODS

Procedures for Animal Experimentation

Pathogen-free fertilized White Leghorn chicken eggs were obtained from Rosenbusch Institute (Buenos Aires). They were incubated at 39°C and 60% relative humidity. Animals were treated according to the Guide for the Care and Use of Laboratory Animals (Institute of Laboratory Animals Resources, Commission of Life Sciences, National Research Council). Embryos were studied every 2 days between the 2nd and the 12th EDs. They were anesthetized by hypothermia, removed from the eggs and staged according to the Hamburger and Hamilton (1951) stages (HH stages). Three sets of embryos were obtained for: (a) whole mount preparations, (b) complete histological serial sections for conventional staining, and (c) serial sections for immunocytochemical staining. Complete embryos (ED2-ED4/HH13-HH23) or brains (ED6-ED12/HH29-HH38) were dissected out in ice-cold 0.1 mol l^{-1} sodium phosphate buffer (pH 7.4), plus 0.9% w/v NaCl (PBS) and then fixed by immersion in 4% paraformaldehyde in PBS at room temperature (RT). The time of fixation varied from 40 minutes (ED2 embryos) to 4 hrs (ED12 brains).

Whole Mount (In Toto) Preparations

Young embryos (ED2-ED4/HH13-HH23) and brains (ED6-ED12/HH29-HH38) (two specimens for each ED) were mounted in toto to be used as references for the construction of 3D OT virtual images. Following fixation, specimens were washed, slightly stained to visualize CNS regions, dehydrated in an ethanol gradient, cleared with propylene oxide and embedded in a synthetic resin. Afterwards, embryos were mounted on well slides.

Complete Serial Histological Sections

After fixation, specimens were washed in PBS, dehydrated in an ethanol gradient, cleared in xylene and embedded in Paraplast™ at 56°C (Product No. 8889-501006. Pellet form). Serial 10 μm thick sections with different spatial orientations were obtained (See Morphometry). They were rehydrated in a decreasing ethanol gradient and stained with hematoxylin and eosine (H-E) or with Toluidine Blue. Then, they were dehydrated and mounted with Histomount (National Diagnostics, Inc. HS-103) on standard slides.

Whole mount embryos and complete serial sections of embryos of defined EDs and HH stages purchased from Carolina Biological Supply Company were also analyzed in this study.

Immunocytochemistry

Sections performed according to different spatial orientations (See Morphometry) were immunolabeled with the primary antibodies listed in Table 1.

Following fixation, a set of specimens, from ED2 to ED12, were dehydrated and embedded in paraffin. Ten μm thick serial sections (three specimens for each ED and orientation) were obtained and collected on gelatinized slides, dried for 1 hour at 37°C and then stored at 4°C. Before immunostaining, sections were deparaffinized, rehydrated, rinsed in PBS and processed for antigen retrieval. Nonspecific binding was blocked by preincubating the sections in 5% normal goat serum (NGS) in PBS with 0.05% Triton X-100 (TX-100) for 1 hour at RT in humidity chamber. These sections were used for immunolabeling with the antibodies directed to Notch1, NeuroD1, βIIITub, Hes5 and NF-M.

Another set of specimens were cryoprotected in 5, 10, and 20% sacarose in PBS (15 min each) and stored for 20 hours at 4°C. Afterwards, they were frozen in a 1:1 (v/v) mixture of 20% sacarose solution and tissue freezing medium (Tissue-Tek OCT Compound, Sakura Finetek Europe, Zoeterwoude, Netherlands). Cryosections (12 μm thick) were obtained (Leica CM 1900, Wetzlar, Germany), collected on gelatinized slides and stored at −20°C until use. These sections were used for immunolabeling with antisynaptotagmin I antibody. Before immunostaining, sections were thawed and rinsed in PBS. Blocking of nonspecific binding and permeabilization were simultaneously performed by preincubation in 5% NGS in PBS containing 0.3% TX-100 for 1 hour at RT in humidity chamber.

For both sets of specimens immunolabeling was performed with primary antibodies diluted in PBS containing 0.5% NGS (See Table 1). Sections were incubated with the primary antibodies for 20 hours at 4°C in humidity chamber. After several rinses in PBS, sections were incubated with secondary antibodies diluted 1:1,000 in PBS for 2 hours at RT in a dark humidity chamber. Sections were then rinsed in PBS and counterstained by a 10 minutes incubation with nuclear dye Hoechst 33342 (B-2261, Sigma) in PBS (dilution 1:1,000) at RT in a dark humidity chamber for histoarchitecture analysis. After rinsing, slides were mounted with polyvinyl alcohol mounting medium with DABCO, antifading (10981, Fluka).

Alexa Fluor 488 goat anti-rabbit IgG (H+L) (A-11008, Molecular Probes) and Alexa Fluor 488 F(ab')2 fragment of goat anti-mouse IgG (H+L) (A-11017, Molecular Probes) were used as secondary antibodies.

Antigen retrieval. Antigen retrieval for Notch1 and Hes5 was performed by treatment with 0.1% TX-100 in PBS for 30 minutes at RT with gentle rotary shaking. Syt retrieval was performed during the incubation in 5% NGS in PBS containing 0.3% TX-100 for 1 hour at RT in humidity chamber. NF-M, βIIITub and NeuroD retrieval was performed by treatment with

TABLE 1. Primary antibodies characteristics

Antibody/species	Supplier/code/lot	Immunogen	Dilution
Rabbit polyclonal antinotch homolog 1, translocation-associated (notch1)	Lifespan biosciences LS-C16928 Lot 6113061	Synthetic peptide CQHSYSSPVDNTPSHQ N-terminal added cysteine Human notch1 intracell. domain (aa 2488-2502)	1:300
Rabbit polyclonal antihairy and enhancer of split 5 (Hes5)	Lifespan biosciences LS-C24205 Lot 7030127	Synthetic peptide SLHQDYSEGYSWC Mouse Hes5 (aa 83-95)	1:100
Rabbit polyclonal antineurod (NeuroD1)	Lifespan biosciences LS-C9245 Lot 8030526	Synthetic peptide DDDQKPKRRGPKKKKM Conjugated to malemide-activated KLH Human NeuroD1 (aa 76-91)	1:100
Mouse monoclonal antineurofilament (160 kDa)	Developmental studies Hybridoma bank 4H6	Chick optic nerve axons	1:50
Mouse monoclonal antineuron specific beta III tubulin [TUJ-1]	Abcam ab14545 Lot 543886	Rat brain microtubules (whole Protein)	1:500
Mouse monoclonal antisynaptotagmin I	Chemicon International MAB5200 Lot 24071317	Rat brain synaptotagmin (whole Protein)	1:200

0.294% sodium citrate, pH 6 for 15 minutes at 95°C. The preceding procedure allows the detection of cytoplasmic NeuroD reactivity [NeuroD(cyt)]. A more drastic NeuroD retrieval (acidic treatment in 0.1% citric acid, pH 2.7 for 15 minutes at 95°C) was performed to reveal NeuroD nuclear reactivity.

Controls. The antibodies used in this paper were used as biomarkers of different cell elements: NE cells bodies, nuclei and processes as well as neuronal perikarya and/or nuclei, developing neurites (dendrites and axons) and synaptic terminals. Negative controls for the primary antibodies were performed by using several chick adult non-neural and nonendocrine tissues. Negative controls for the secondary antibodies were performed on OT sections of each ED processed without preincubation with primary antibodies. Neither kind of negative control exhibited detectable fluorescence.

Definition of Developmental Stages

Developmental stages were defined by using three sets of data: (a) qualitative histogenetic features (b) immunolabeling pattern, and (c) morphometry (quantitative parameters, construction of 2D Maps and 3D OT virtual images). These data were analyzed with an image processing device (Carl Zeiss, Oberkochen, Germany) consisting of an Axioplan 2 imaging optical epifluorescence microscope with an Axiocam HR color digital scanner and a computer equipped with the following software: Axiovision™ (Carl Zeiss, Oberkochen, Germany), MATLAB™ (The MathWorks, Inc., Natick, Massachusetts), 3ds Max™ (Autodesk, San Rafael, CA), CorelDRAW™ (Corel Corporation, Ottawa), Photoshop™ (Adobe Systems, San Jose, CA) and software implemented by our own group (IGTB, UF) (Firka et al., 2004; González et al., 2007). Brightness and contrast levels of digital images were adjusted by using the same set of specifications for images obtained at the same magnification.

Morphometry

Histological sections with different orientations were used depending on the ED, since the OT developmental gradient axis orientation changes during development (LaVail and Cowan, 1971a; Itasaki et al., 1991; Matsuno et al., 1991; Scicolone et al., 1995). During the early stages (up to ED6) the OT anatomical longitudinal axis almost exactly coincides with cph-cd axis and slightly deviates from the developmental gradient axis orientation. Afterwards, the OT "rotates" with respect to the neural tube axis and the anatomical longitudinal axis extends from the site where the retinal axons enter the OT to the caudal end. Sections with these orientations closely approximate the developmental gradient axis. Planes of section showing the maximal difference in tissue differentiation between both OT ends were considered as those that best approximate the developmental gradient axis position. For simplicity, planes of section coinciding with the developmental gradient axis are named as cephalic-caudal (cph-cd) sections and planes of section perpendicular to the developmental gradient axis are named as dorsal-ventral (d-v) sections.

Records of Quantitative Data

Estimation of mitotic NE cells density. Mitotic cells were identified in H-E or basophilic staining. Given that the section thickness (10 μm) is larger than the mean mitotic cell diameter, an adaptation of the stereological optical disector method (Coggeshall and Lekan, 1996) was used to estimate the number of mitotic NE cells. Highly magnified images −1000 X at a final digital amplification of 5000 X–were used to obtain several focal planes from each section. Once a mitotic cell profile was identified and computed in a given focal plane it was no longer computed in the following planes. With regards to the mitotic cell fragments only those located on the upper surface of the section were computed. Those located on the lower surface were not considered. The density of mitotic NE cells was expressed in terms of number of mitotic NE cells/100 μm^2 of the ILM surface.

Estimations of mitotic NE cells density were performed on sections: (a) coinciding with the cph-cd (developmental gradient) axis, (b) located halfway along the d-v axis and (c) perpendicular to the inner limiting membrane (ILM). Four midbrains, from ED2 to ED10, were studied on each ED. Values of density computed on four adjacent sections were averaged for each OT. Estimations of mitotic NE cells density were performed along selected intervals of the cph-cd axis corresponding to each DS or each transitional stage. The values of mitotic NE cells density were analyzed as a function of both EDs and DSs.

Quantitative data on the OT growth and its architectural organization. Values of thickness of the entire OT radial axis and of each radial zone were recorded by using the

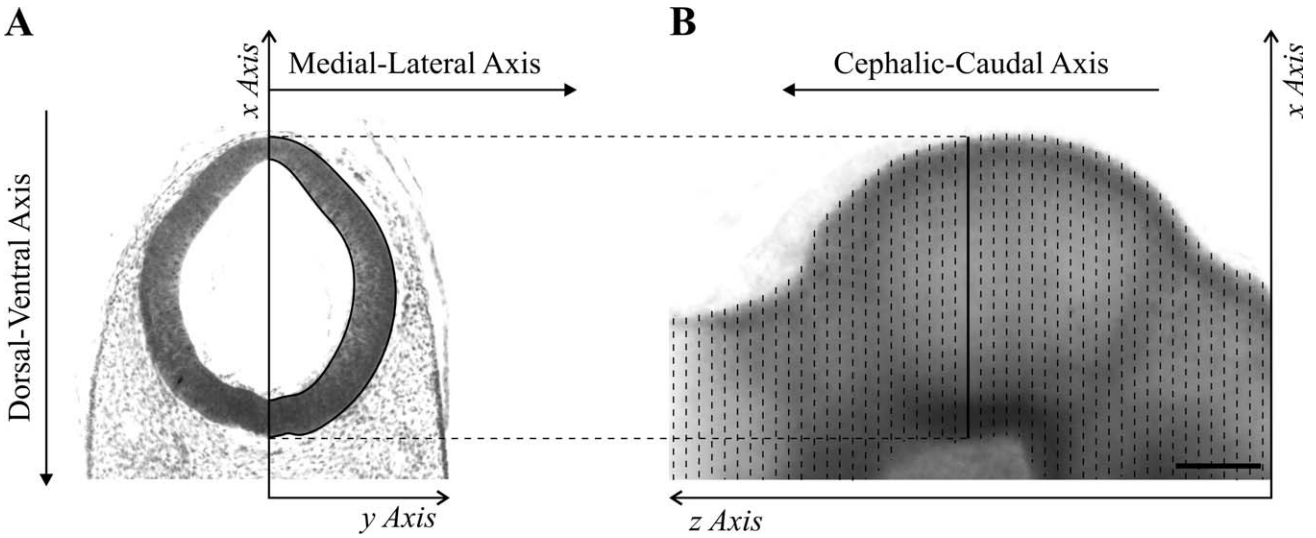

Fig. 1. Construction of an OT 3D virtual image by the ordered stacking, along the "*z*" axis, of a complete series of 2D maps of dorsal-ventral OT sections. (**A**) Dorso-ventral midbrain section (ED2, HH14). The ILM and OLM contours were outlined on the right side of the section. The "*x*" axis corresponds to the sagital plane projection (midline) and the "*y*" axis to the medial-lateral axis. (**B**) Right lateral view of a whole-mounted midbrain (ED2, HH14). "*x*" and "*z*" axis are shown. Dotted vertical lines specify the correct position of each 2D map along the "*z*" axis. The full line specifies the correct position of the 2D map shown in A Bar: 100 μm.

multiple calipers tool of the Axiovision software. A pair of values was recorded for each interval of the cph-cd axis corresponding to each DS: one of them corresponding to the cephalic end and the other to the caudal end of each DS interval. Four adjacent sections were analyzed from each OT corresponding to each ED. These values were averaged and used as references to draw a dynamic and continuous 2D spatial diagram illustrating the evolution of the OT architectural organization as a function of the DSs.

Statistical analyses. Data on the OT growth and its architectural organization were analyzed statistically using the Statistics Toolbox™ (The MathWorks, Inc. MATLAB, Natick, Massachusetts). Data were analyzed with a one-way analysis of variance (ANOVA) followed by multiple comparison of means using Tukey-Kramer post-hoc test. A value of $P < 0.01$ was considered as statistically significant. Data on NE cells proliferation were processed with an automatic clustering algorithm (clusterdata, MATLAB™) to evaluate the presence of clusters of values. Statistical significance of the differences amongst clusters was then corroborated with a one-way ANOVA followed by Tukey-Kramer post-hoc test.

Construction of 2D Maps of DS Topographic Distribution

At any ED, successive areas corresponding to different DS can be seen distributed along the OT cph-cd axis. Complete series of 2D maps of the different DSs areas distribution were constructed by using complete serial histological sections of different EDs and HH stages. Six (3 cph-cd and 3 d-v) serial sections were obtained at each ED. Images (50×)

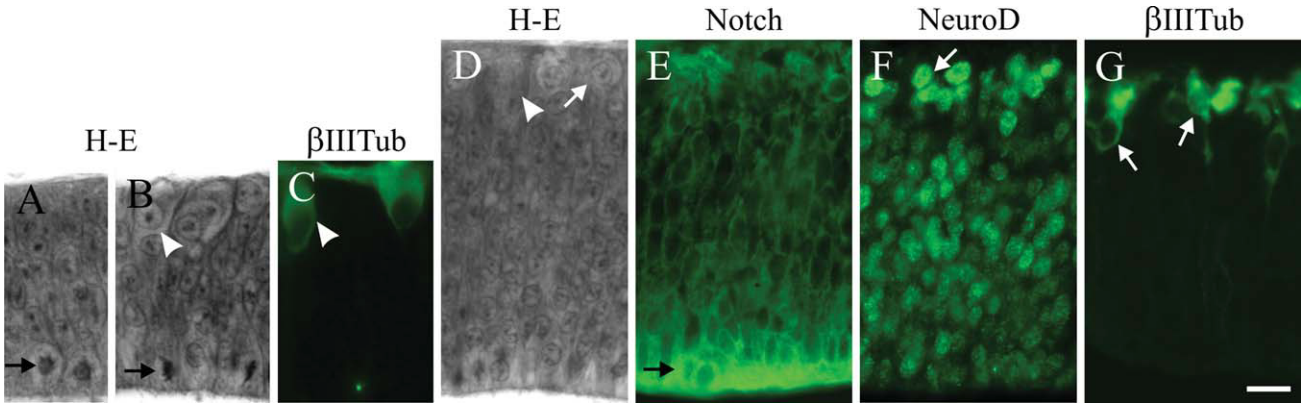

Fig. 2. Radial organization and immunocytochemical patterns during DS1. (**A**) Lateral region of the optic tectum (ED2, HH14). (**B**, **C**) Dorsal region of the optic tectum (ED2, HH14). (**D–G**) Lateral region of the OT (ED4, HH23). Black arrows point to mitotic NE cells; they show intense Hes+ (not shown) and Notch+ cytoplasm (E); interphasic NE cells exhibit Notch+ cytoplasms and Notch– nuclei (E). Arrowheads point to Mes5 neurons; they display βIIITub+ cytoplasm (C). White arrows point to the future TCC1 neurons located at the premigratory zone; they display a nuclear NeuroD reactivity that increases towards the OLM (F); upon arrival the premigratory zone they show βIIITub+ perikarya. B, C correspond to dorsal-ventral sections; the others correspond to cephalic-caudal sections. All figures at the same magnification. Bar: 10 μm. [Color figure can be viewed in the online issue, which is available at wileyonlinelibrary.com.]

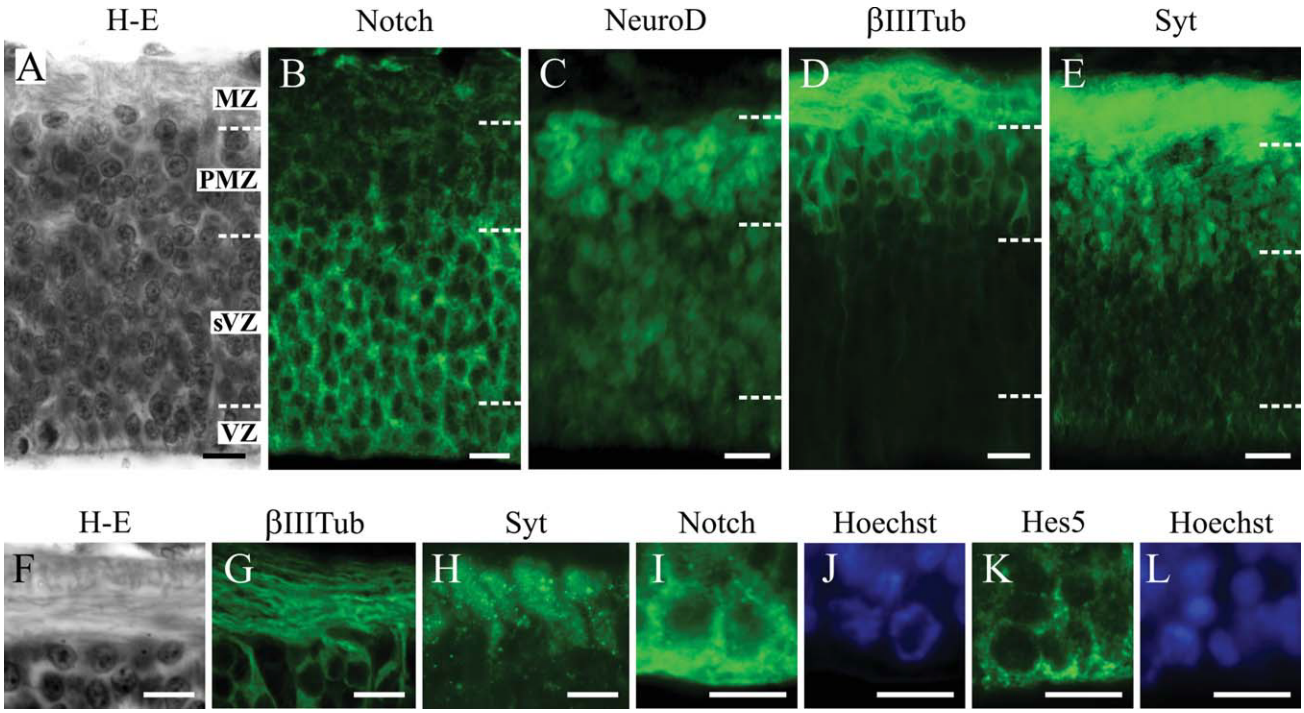

Fig. 3. Radial organization and immunocytochemically patterns during the DS2 (ED6, HH29). (**A**) Axial positions of the four immunocytochemically defined radial zones. (**B**) The GZ (VZ+sVZ) shows densely packed NE cells with Notch+ cytoplasm and Notch– nucleus; they typically lack βIIITub and Syt reactivity. Some slight NeuroD+ nuclei intermingle with the NE cells. (**C–E**) The PMZ is mainly occupied by the future TCC1 (NeuroD+ nuclei, βIIITub+ perikarya and Syt+ somata) neurons. βIIITub+ and Syt+ neurites from these neurons invade the MZ. (**F–H**) The marginal zone and the superficial PMZ. The MZ is invaded by βIIITub+ and Syt+ neurites from the future TCC1 neurons located at the PMZ. (G) (a dorsal-ventral section) shows how the basal processes of the TCC1 neurons bend and run as tangential axons following a dorsal-ventral direction. (H) (a cph-cd section) shows parallel fascicles of these future axons. (**I–L**) Show the VZ. Mitotic NE cells display strong Notch+ (I) and Hes5+ (K) cytoplasm. (J, L) show their corresponding Hoechst chromosome labeling. (A–C,H) cph-cd sections; (D–G) d-v sections. Bars: 10 μm. [Color figure can be viewed in the online issue, which is available at wileyonlinelibrary.com.]

of each histological section were used to outline, by means of the Bézier tool of the CorelDRAW™ software, the complete contour of the ILM and the outer limiting membrane (OLM) of both tectal hemispheres (Fig. 1). Afterwards, areas corresponding to the different DSs were demarcated over each section contour. The histogenetic differences between adjacent/successive DSs appear as sharp or gradual changes along the cph-cd axis. In the first case, short transitional zones separate two consecutive DSs and a line in the middle of the transitional zone is used as a landmark between them. In the second case, wide transitional zones expand between two successive DSs; in these cases, the transitional zone is indicated in the 2D map and described in the text as a transitional stage (TS) between the two consecutive DSs.

Construction of 3D Maps of DS Topographic Distribution

Three dimensional maps of the distribution of DSs areas were constructed with the 3ds Max™ software. Each 2D map is defined by the "*x*" axis (midline) and the "*y*" axis (medial-lateral axis) (Fig. 1A). Each 3D reconstruction was obtained by the ordered stacking of a series of 2D maps over the "*z*" axis (perpendicular to the planes of sections) (Fig. 1B). To obtain reliable 3D OT reconstructions, images of whole mount preparations were used as reference to locate every 2D map within the contour of a real specimen and at the correct position over the "*z*" axis (Fig. 1A,B). The number of 2D maps that had to be assembled to obtain a reliable 3D map differs according to the OT size which, in turn, depends on the ED and HH stage.

Nomenclature. The nomenclature introduced by Scicolone et al. (1995) about the developing OT lamination is used in this paper. The essentials of that nomenclature are preserved. However, significant modifications and reinterpretations of the OT development are presented. The definition and the rationale of the notion of transient cell compartment (TCC) are given in Scicolone et al. (1995). See Supporting Information 1: About the nomenclature of the developing chick OT organization.

RESULTS

Optic Tectum Developmental Stage Characterization

Developmental stages are characterized as typical set of changes that take place as function of both the ED and the position along cph-cd axis. Significant changes in structural complexity are taken as landmarks between temporally successive/spatially adjacent DSs. Although DSs correlate with EDs and HH stages, several different DSs coexist at a given ED or HH stage. Correspondingly, a given DS can be found in successive EDs, although at different positions along the cph-cd axis.

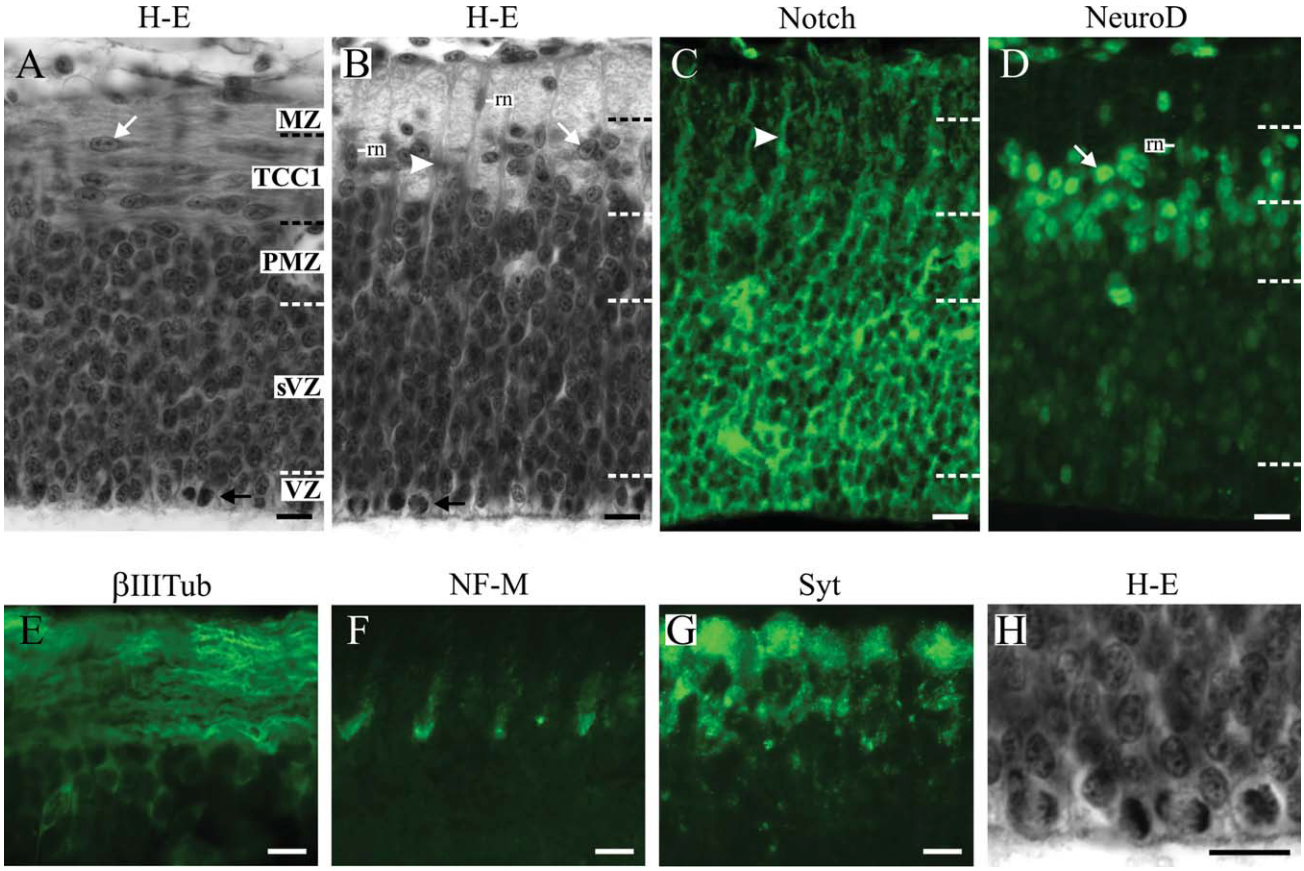

Fig. 4. Radial organization and immunocytochemical patterns during the DS3 (ED6, HH29). (**A**,**B**) Radial position of the five immunochemically defined radial zones; (A) d-v section; (B) cph-cd section, illustrates the periodic organization of the NE cell basal processes. White arrow: TCC1 neurons already detached from the PMZ; m: small fusiform neurons attached to the NE cell basal process. (**C**) The GZ (VZ plus sVZ) shows the honey comb-like pattern of Notch+ NE cell bodies with Notch- nuclei. Arrowhead: Radial Notch+ NE cell basal processes; they run through the PMZ, the TCC1, the MZ and arrive the OLM [see also (B)]. (**D**) Round NeuroD+ nuclei characterize the superficial PMZ. White arrows: intensely reactive rounded neurons detached from the PMZ and forming the TCC1 (see also B and C); m: small fusiform neurons crossing the TCC1 (see also B). (**E**)–(**G**) Detail of the MZ, TCC1 and PMZ. (E) βIIITub+ axon fascicles from the TCC1 neurons run tangentially in d-v sections. (F) NF-M+ axon fascicles from the TCC1 neurons arrange as periodic and parallel fascicles in cph-cd sections. (G) Syt+ axon fascicles from the TCC1 neurons arrange as parallel fascicles (cph-cd section). The older NF-M+ axons, presumably corresponding to type I SGC neurons, lay deeply in the MZ while the younger Syt+ axons, probably corresponding to the other SGC neurons, have a more superficial position. (**H**) Clusters of mitotic NE cells are abundant during DS3. The cph-cd sections (B,C) and (F,G) reveal the periodic organization of the NE cells basal processes and of the TCC1 axon fascicles. Bars: 10 μm. [Color figure can be viewed in the online issue, which is available at wileyonlinelibrary.com.]

Developmental Stage 1 (DS1)

NE stage. Emergence of the first postmitotic neurons. The OT wall is a single layered cylindrical neuroepithelium composed of thin NE stem cells extended radially from the ILM to the OLM (Fig. 2A). The mitotic NE cells form the ventricular zone (VZ) (Fig. 2A,B,E). The 1st neuronal cohort, the future Mes5 sensory neurons of the mesencephalic trigeminal nucleus, appears along the dorsal midline between ED2-ED4 (Fig. 2B,C). The 2nd cohort, the future large efferent neurons, appears over the entire OT wall (Fig. 2D,F,G) from ED3.5-ED4 onwards. They are born near the ILM and move to the outermost zone forming an incipient premigratory zone (PMZ). Developmental stage 1 begins as a single layered neuroepithelium and evolves until the appearance of the PMZ composed of the first postmitotic neurons (Fig. 15).

Developmental Stage 2 (DS2)

Emergence of the marginal zone (MZ), delimitation of the PMZ and the generation zone (GZ). The OT wall develops a superficial fibrous MZ (Fig. 3A). The cellular zone is composed of a deep GZ and a superficial PMZ. The GZ is composed of a VZ (a single row of mitotic NE cells) (Fig. 3I–L) and a subventricular zone (sVZ, i.e., a thick layer of densely packed interphasic NE cell bodies (Fig. 3A,B). During DS2 the PMZ (Fig. 3A,C–E) thickens by the addition of neurons of the 2nd cohort. The outermost of these early differentiating premigratory neurons generates a neurite (Fig. 3A,D–H) that run tangentially following the d-v axis. These neurites, together with the outermost segment of the NE cell basal processes, form the fibrous MZ. During DS2 a 3rd cohort of small

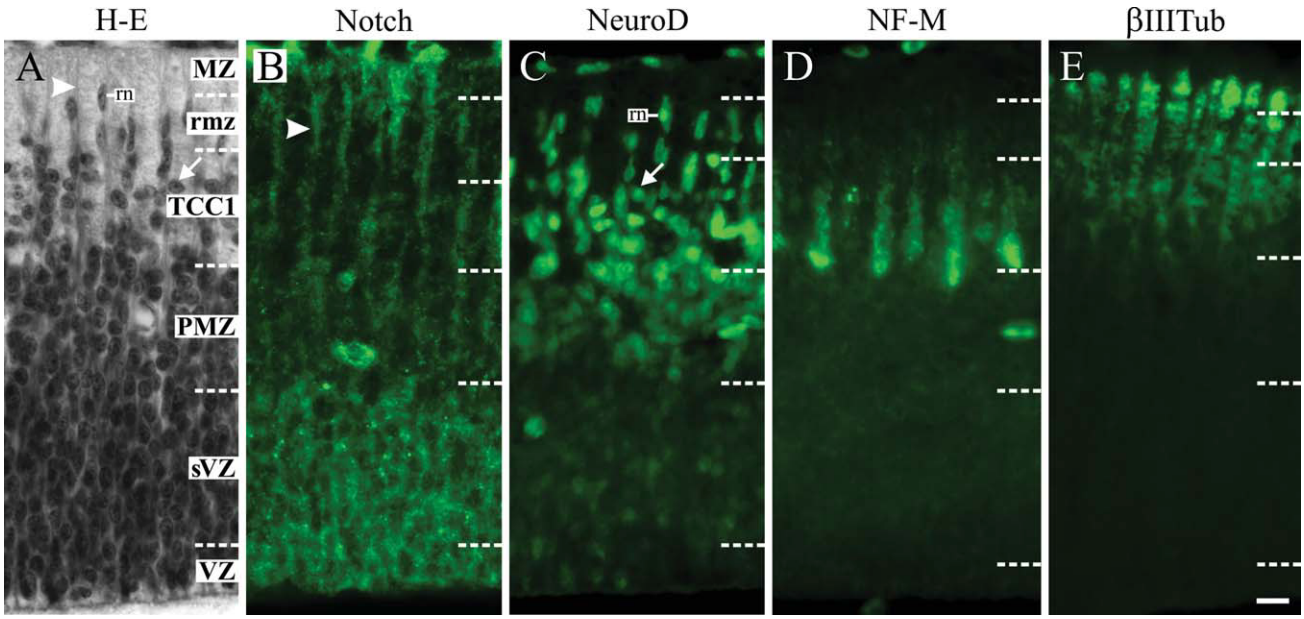

Fig. 5. Radial organization and immunocytochemical patterns during the TS3-4 (ED6, HH29). (**A**) Radial position of each immunochemically defined radial zone. Arrow: TCC1 neuron; Arrowhead: NE cell basal process; m: radially migrating neuron (3rd cohort); rmz: radial fusiform neurons migrating beyond the TCC1 and invading the deep MZ (See also **C**). (**B**) The GZ (VZ+ sVZ) shows its typical Notch reactivity. Arrowhead points to radial and periodical Notch+ NE cell basal processes extended up to the OLM. The GZ also displays some slightly stained NeuroD+ nuclei (probably 3rd neuronal cohort) (C) and lack NF-M and βIIITub reactivity (**D**,**E**). (C) The TCC1 neurons display intense NeuroD+ nuclei (arrow) and slight βIIITub labeling (E). The PMZ neurons (probably 3rd neuronal cohort) show less intense NeuroD reactivity. m: the small fusiform, probably migrating neurons (3rd cohort) also show intense NeuroD+ nuclei (see also A). (D,E) Illustrate the periodical organization of the TCC1 neuron axon fascicles. The older NF-M+ axons run deeply while the younger βIIITub+ ones run superficially. All images correspond to cph-cd sections. Bar: 10 μm. [Color figure can be viewed in the online issue, which is available at wileyonlinelibrary.com.]

neurons appears intermingled with the NE cell bodies at the sVZ (Fig. 3C). Developmental stage 2 displays the following radial organization: (1) a GZ (VZ + sVZ); (2) a PMZ and (3) a MZ composed of the first growing neurites (Fig. 15).

Developmental Stage 3 (DS3)

Emergence of TCC1. Neurons of the 2nd cohort detach from the PMZ and begin the TCC1 formation between the PMZ and the MZ. The early TCC1 is composed of medium-sized fusiform neurons tangentially oriented along the d-v axis (compare Fig. 4A,B) with similarly oriented neurites (future axons) (compare Fig. 4A,G with B,F,H). These axon fascicles run superficially along the 10 μm thick parallel corridors limited by periodic palisades of NE cells (Fig. 4B,C). As the TCC1 neurons detach from the PMZ this zone is gradually occupied by the 3rd cohort of neurons. During the late DS3 these last neurons attach to NE cell basal processes and transform into small fusiform radially oriented neurons that migrate across the TCC1 and invade the MZ (Fig. 4B,D). Neurons of this cohort are probably born between ED5.5 (HH27) and ED10 (HH36) and originate several subpopulations of local circuit neurons (LaVail and Cowan, 1971b; Puelles and Bendala, 1978). During DS3 clusters of mitotic NE cells abound at the VZ (Fig. 4E). Developmental stage 3 displays the following radial organization: (1) the GZ (VZ plus sVZ), (2) the PMZ, (3) the TCC1 (also a zone of radial migration), and (4) the MZ (Fig. 15).

Transitional Stage 3-4 (TS3-4)

The fusiform radially migrating neurons (3rd cohort) surpass superficially the TCC1 and locate between the MZ and the TCC1 (Fig. 5A,C). The close attachment of these migrating neurons to the NE cell basal processes reveals the 10 μm periodicity of the NE cells (Fig. 5C). This periodicity is also revealed by the Notch+ NE cell basal processes and by the orientation of the TCC1 neuron axon fascicles (Fig. 5B,D,E). The PMZ and GZ remain almost unchanged. The TS3-4 displays the following radial organization: (1) the GZ (VZ + sVZ), (2) the PMZ, (3) the TCC1, (4) a zone of radial migration, superficial to the TCC1, and (5) the MZ (See Fig. 15).

Developmental Stage 4 (DS4)

Emergence of the TCC2. The small radially migrating neurons (3rd cohort) surpass the TCC1 and invade the deep MZ. Once a critical mass of them arrive the subpial region, they detach from the NE cells, transform into round- shaped neurons and form a new compartment, the TCC2, between

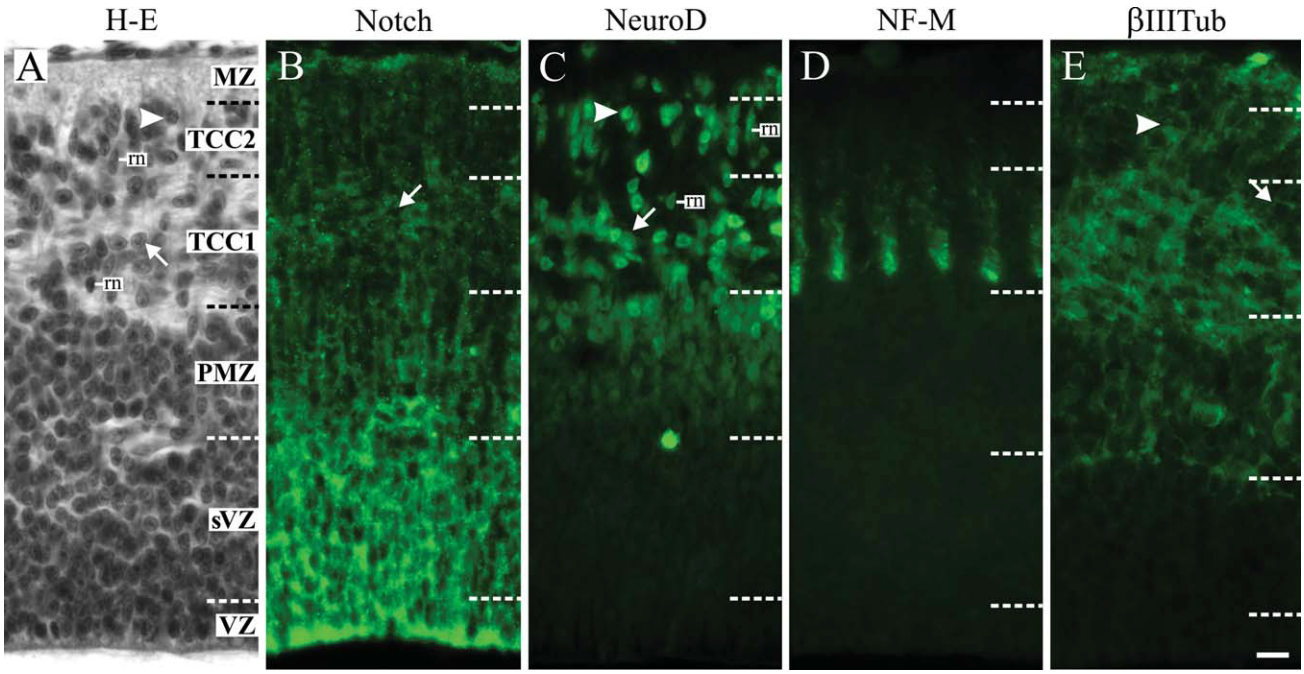

Fig. 6. Radial organization and immunocytochemical patterns during DS4 (ED6, HH29). (**A**) Radial position of each immunochemically defined zone. The TCC2 appears between the MZ and the TCC1. Arrow: differentiating TCC1 neurons (2nd cohort); Arrowhead: rounded postmigratory TCC2 neuron (3rd cohort); m: fusiform radially migrating neuron (3rd cohort). (**B**) The GZ (VZ+sVZ) shows its typical Notch labeling. It is particularly intense at the VZ occupied by mitotic NE cells. The Notch labeling reveals the NE cell periodicity. Some differentiating TCC1 neurons resume a slight cytoplasmic reactivity (arrow). The GZ typically lacks NeuroD, NF-M, βIIITub and Syt (not shown) reactivity. (**C**) Although with different intensity, NeuroD+ nuclei characterize premigratory neurons (PMZ), differentiating TCC1 neurons (2nd cohort), migrating neurons and TCC2 neurons (3rd cohort). (**D**) Illustrates the parallel and periodic organization of the NF-M+ TCC1 neuron axon fascicles. They also display Syt labeling (not shown). (**E**) The βIIITub reactivity localizes at the perikarya of the premigratory neurons (PMZ), the differentiating TCC1 neurons (arrows) and some rounded TCC2 neurons (arrowhead). A slight reactivity is also present at the MZ neuropile. (B, C, D) cph-cd sections. (A, E) d-v sections. Bar: 10 μm. [Color figure can be viewed in the online issue, which is available at wileyonlinelibrary.com.]

the subpial MZ and the TCC1 (Fig. 6A,C,E). By ED6, the TCC2 occupies a small cup-shaped area at the lateral aspect of the OT cephalic pole where the retinal ganglion cell (RGC) axons enter the OT. This is the zone of maximal development (ZMD) (Fig. 16). The TCC2 formation is almost simultaneous with the RGC axons ingression and invasion. Between ED6-ED10 the TCC2 thickens along the radial axis and expands over the tangential plane. When the rounded postmigratory TCC2 neurons detach from the NE cells basal processes the periodicity of the migrating neurons is no longer observed. During DS4, the differentiating TCC1 neurons increase in size and expand between the TCC2 and the PMZ (Figs. 6A,B,C,E). Small radially migrating neurons of the 3rd cohort are seen "in transit" through the TCC1. During DS4 and TS4-5 the TCC1 shows a complex composition: (a) it is the postmigratory zone for the TCC1 neurons (2nd cohort), (b) it behaves as migratory zone for the 3rd neuronal cohort, and (c) it is a pathway for the tangential TCC1 neurons axon fascicles (precursor of the SAC). As judged by their size and NeuroD labeling, the outermost PMZ neurons probably correspond to the 2nd cohort while the innermost likely belong to the 3rd cohort. Rows of mitotic NE cells are present along the VZ. This intensive proliferation explains the thickening the sVZ and the PMZ undergo during TS4-5. Developmental stage 4 displays the following radial organization: (1) the GZ (VZ + sVZ), (2) the PMZ, (3) the TCC1, (4) the TCC2, and (5) the MZ (Fig. 15).

Transitional Stage 4-5 (TS4-5)

Early TCC3 formation. The TCC3 formation begins by ED8 when some fusiform radially migrating neurons surpass the TCC2, enter the deep region of the MZ and transform into rounded, presumably postmigratory, neurons with spherical nuclei (Fig. 7A). During TS4-5 every TCC thickens due to an intensive radial migration (Fig. 15). The PMZ undergoes a remarkable thickening implying that neurons are born at a rate that exceeds the rate of radial migration. Although the radial organization remains almost unchanged (Fig. 15), the pattern of immunolabeling changes significantly (Fig. 7).

Developmental Stage 5 (DS5)

TCC3 formation, delamination of TCC1 into C "SGC" and C "SGP" and appearance of the C "SAC." During DS5 (Fig. 8): (1) More neurons invade the deep region of the MZ which

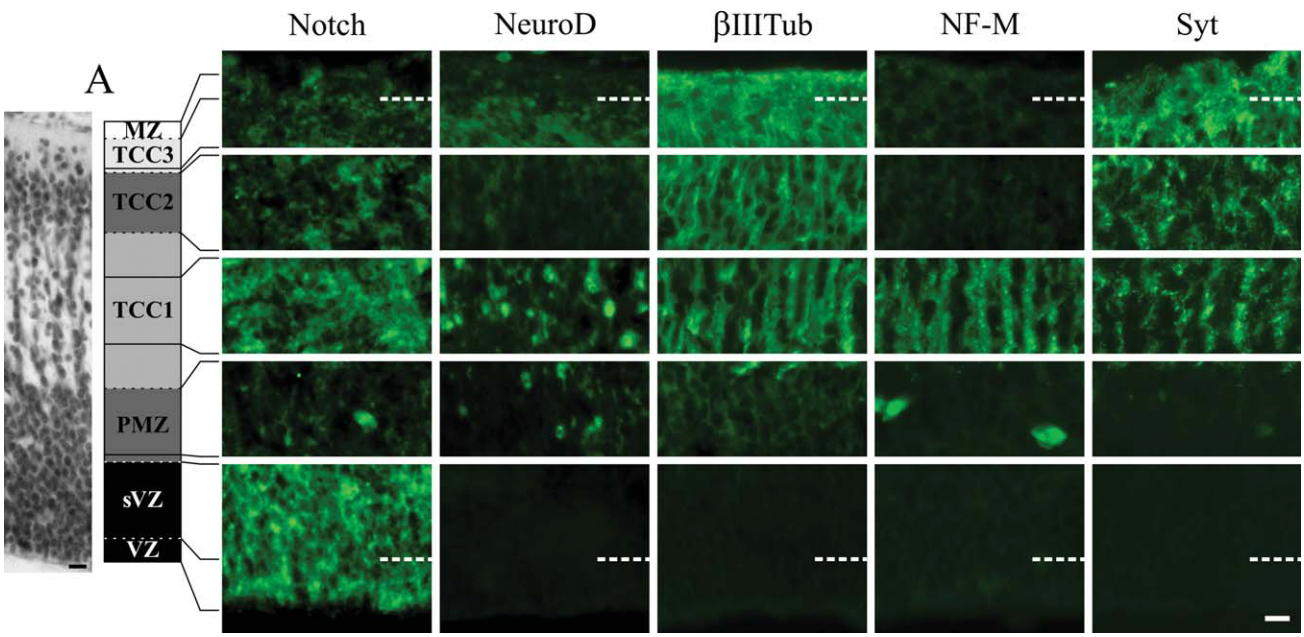

Fig. 7. Radial organization and immunocytochemical patterns during TS4-5 (ED8, HH34). The micrographs illustrate the immunochemical pattern of each TCC (horizontally) and the radial pattern of expression of each antibody (vertically). (**A**) Hematoxylin-Eosin staining and schematic representation of the immunochemically defined radial organization. An incipient TCC3 appears between the MZ and the TCC2. Dotted lines indicate the limits between adjacent compartments. Full lines indicate the zone of each compartment corresponding to the horizontal series of micrographs. The MZ is now a thin βIIITub+ and slightly Syt+ cell-free layer occupied by the future SO axons. The TCC3 shows preferentially radial βIIITub+ and irregular Syt+ neurites. Slight irregularly distributed small Notch+ patches and slight homogeneous NeuroD+ reactivity characterize the TCC3. The TCC2 shows a honey comb-like pattern of βIIITub+ cell bodies and radially oriented neurites, a network of Syt+ neurites and Notch+ neuropile patches and some few neuronal bodies (according to Hoechst staining). The TCC1 displays the periodic pattern of βIIITub+, NF-M+ and Syt+ axon fascicles and clusters of differentiating neurons with NeuroD+ nuclei. Most of them resume the cytoplasmic Notch reactivity. The PMZ shows slight βIIITub+ neuronal bodies with slight NeuroD+ nuclei. The NE cells bodies of the GZ still display intense Notch labeling. All images, except the Notch column, correspond to cph-cd sections. Bars: 10 μm. [Color figure can be viewed in the online issue, which is available at wileyonlinelibrary.com.]

becomes thinner while the TCC3 thickens. The cell-free superficial MZ corresponds to the stratum opticum (SO). (2) Many neurons become postmigratory upon arrival the TCC2 thickening this TCC. (3) The parallel axon fascicles from the large TCC1 neurons grow through the central zone of the TCC1. These fascicles, almost deprived of neurons, are now recognized as the C "SAC." (4) The C "SAC" segregates the large TCC1 neurons into a superficial population, the C "SGC," below the TCC2, and a deep population, the C "SGP," above the PMZ. Thus, during DS5 the TCC1 disappears as a distinct zone and transforms into three different compartments: "SGC," "SAC," and "SGP." (5) Rows of small fusiform neurons (3rd cohort), attached to the NE cell basal processes, continue migrating across the C "SAC" (Fig. 8A). (6) Given that the NE cells proliferation decreases but the radial migration intensely continues, the PMZ weakens while the TCC2 and TCC3 thicken (Fig. 8A). Developmental stage 5 displays the following radial organization: (1) GZ (VZ plus sVZ), (2) PMZ (3) C "SGP", (4) C "SAC", (5) C "SGC", (6) TCC2, (7) TCC3, and (8) SO (Fig. 15).

Transitional Stage 5-6 (TS5-6)

Early TCC4 formation. During TS5-6 a subset of the 3rd neuronal cohort migrates through the TCC2 towards a more superficial position. They form coherent rows of radially oriented fusiform neurons attached to the NE cell processes (Fig. 9). They initially form a discontinuous, poorly defined, layer of fusiform neurons below the TCC3 which is composed of round-shaped and horizontally oriented neurons diffusely distributed below the SO (Fig. 9, left zone). As an increasing number of neurons traverse the TCC2 towards this new position a new compartment, the TCC4, emerges (Fig. 9, right zone). Figure 9 illustrates the TCC4 formation as a process of TCC2 cellular segregation into two new neuronal compartments separated by a zone of low neuronal density, the inter TCC4-2 fibrous band (future C "h"). During TS5-6 the C "SGC", C "SAC", and C "SGP" are better defined. The NE cells proliferation declines, the radial migration across the C "SAC" continues and the PMZ weakens (Fig. 15).

Developmental Stage 6 (DS6)

Delamination of TCC2 into TCC4, C "h" and C "i-j." During DS6 (Fig. 10) the TCC2 segregates

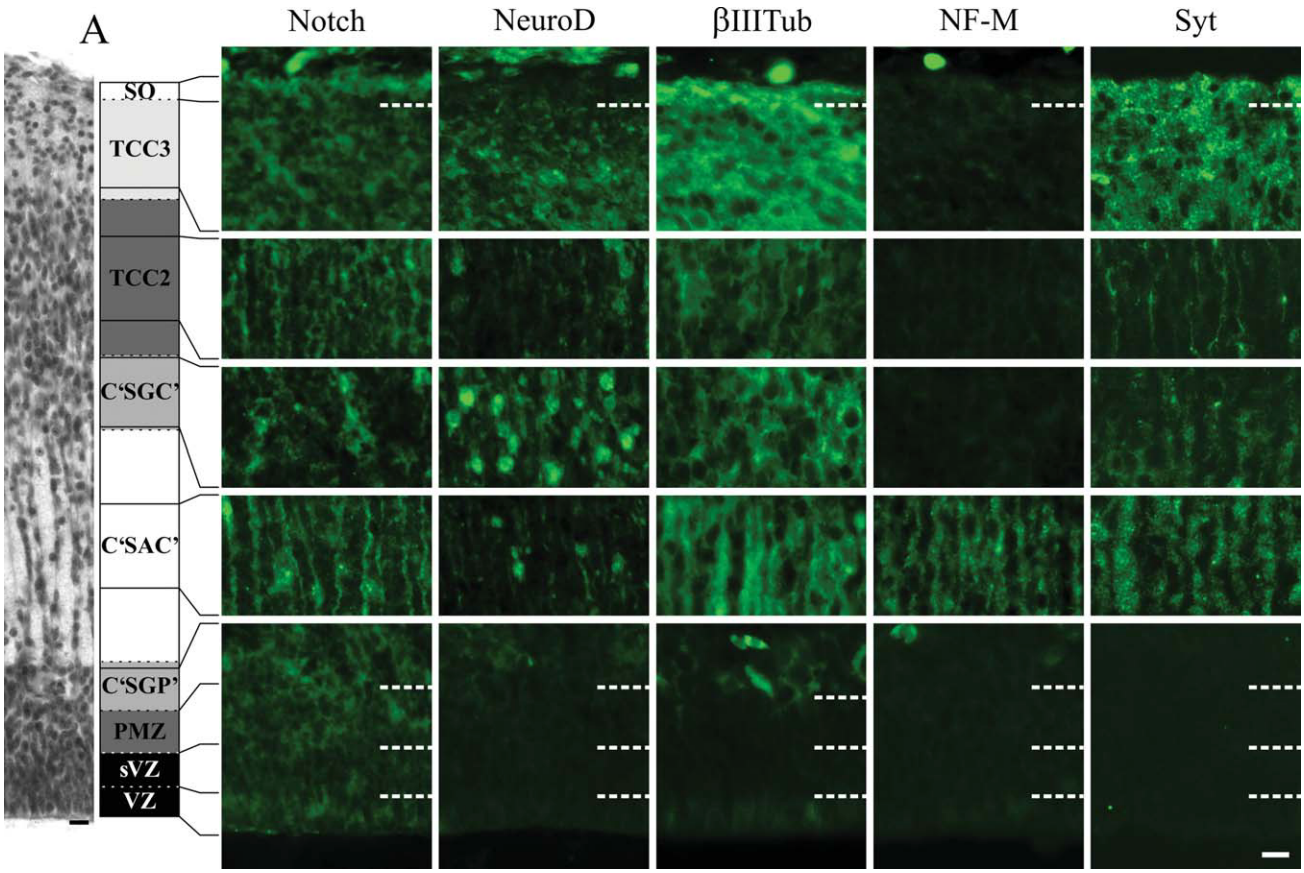

Fig. 8. Radial organization and immunocytochemical patterns during DS5 (ED10, HH36). The micrographs show the immunochemical pattern of each TCC (horizontally) and the radial pattern of expression of each antibody (vertically). (**A**) Hematoxylin-Eosin staining and schematic representation of the OT radial organization. The TCC1 is replaced by the C "SGC," "SAC" and the "SGP," TCC2 and TCC3 thickens while the PMZ and GZ weaken (compare with Fig. 7). Dotted lines indicate the limits between adjacent compartments. Full lines indicate the zone of each compartment corresponding to the horizontal series of micrographs. An incipient SO displays slightly Notch+, βIIITub+ and Syt+ axon fascicles. The TCC3 displays βIIITub+ perikarya, some NeuroD+ nuclei and a Syt+, βIIITub+ and NeuroD+ neuropile with a slight and diffuse Notch reactivity. The TCC2 shows some βIIITub+ perikarya, some NeuroD+ nuclei, Notch+ NE cell basal processes and radial Syt+ neurites. The C "SGC" neurons display NeuroD+ nuclei and βIIITub+ perikarya; some of them show Notch+ perikarya. They are surrounded by a diffuse Syt+ neuropile. The C "SAC" is characterized by βIIITub+, NF-M+ and Syt+ parallel axon fascicles with some few NeuroD+ neurons corresponding to migrating interneurons (3rd cohort). Radial Notch+ NE cells basal processes can still be observed. The C "SGP" neurons show a slight βIIITub labeling. The Notch reactivity of NE cells bodies significantly decreases at the GZ. All images correspond to cph-cd sections. Bars: 10 μm. [Color figure can be viewed in the online issue, which is available at wileyonlinelibrary.com.]

into new compartments. A subset of TCC2 neurons migrates superficially forming the TCC4 below the TCC3. A fibrous band of low neuronal density, named as "inter TCC3-4 layer," separates these TCCs. The remaining TCC2 neurons retain their original position and, another band of low neuronal density, the "inter TCC4-2 layer," appears between the TCC4 and these remaining TCC2 neurons. From DS6 onwards, the inter TCC4-2 fibrous layer and the remaining TCC2 neurons are designated as C "h" and C "i-j" respectively, because together they can be topographically identified as precursors of the definitive layers "h," "i," and "j" of the SGFS. During DS6 the inter TCC3-4 and the inter TCC4-2 (C "h") fibrous layers remarkably thicken revealing an intensive neuritogenesis which probably corresponds to dendrite growth (Fig. 10). The immunochemical labeling shows that the C "i-j" is composed of two distinct regions: a C "i," mainly characterized as a dense neuronal layer, and the C "j," characterized by an abundant neuropile (Fig. 10). The C "SGC" and the C "SGP" display large differentiating neurons with similar immunocytochemical pattern. A thin layer of neurites, the future C "SFP," appears between the C "SGP" and the PMZ. The C "SGP" and the C "SFP" will form the SGFP. During DS6 the NE cells proliferation, the PMZ thickness and the number of neurons migrating across C "SAC" significantly decrease. Most of the GZ cells no longer correspond to NE stem cells. Developmental stage 6 displays the following radial organization: (1) The GZ (VZ plus a thin sVZ), (2) a thin PMZ, (3) the C "SFP," (4)

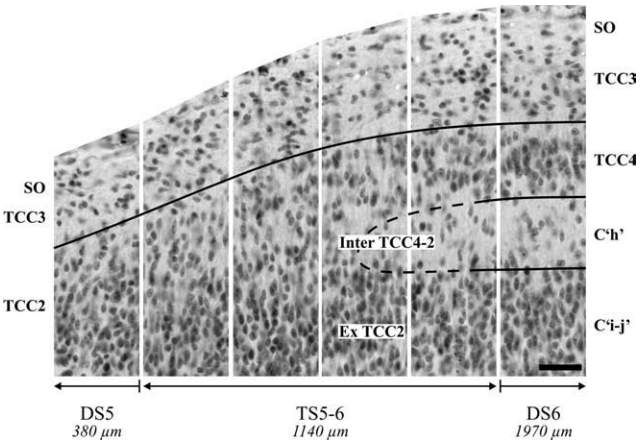

Fig. 9. Transitional changes between DS5 and DS6. The TS5-6 characteristics are documented by only four partial images of the transitional zone that covers a distance of 1140 μm of the section. The TS5-6 zone is "preceded" by a DS5 zone that occupy around 400 μm of the developmental gradient axis (on the left) and is "followed" by a larger DS6 that linearly takes around 2000 μm along the developmental gradient axis (on the right). The images where obtained from an OT (ED12, HH38) cut along the developmental gradient axis. Bar: 25 μm.

the C "SGP," (5) the C "SAC," (6) the C "SGC," (7) the C "i-j," (8) the fibrous C "h," (9) the TCC4, (10) the inter TCC3-4 fibrous layer, (11) the TCC3, and (12) the SO (Fig. 15).

Transitional Stage 6-7 (TS6-7)

During TS6-7 the OT structure is better defined: (1) the SO thickens due to the arrival of more RGC axons; (2) The TCC3 and TCC4 enlarges and there is a period along which the boundary between both TCCs, i.e., the inter TCC3-4 fibrous layer, is transiently vanished. The images suggest that a redistribution of neurons through the inter TCC3-4 layer transiently blur the boundary between both TCCs (Fig. 11); (3) The fibrous C "h" enlarges considerably and is better defined; (4) the C "i-j" weakens confirming that many migrating neurons are still leaving the C "i-j"; (5) the large C "SGC" neurons increase in size and are separated by a growing neuropile. (6) The C "SGP" and C "SFP" become better defined; they will form the SGFP (Fig. 15). (7) The NE cells proliferation ceases, the GZ transforms into a pseudostratified-like epithelium and the PMZ almost completely disappears.

Developmental Stage 7 (DS7)

Establishment of the basic OT cortical organization. By ED12 (HH38) the ZMD reaches the DS7 (Figs. 12 and 16). Developmental stage 7 is characterized by a remarkable increase in thickness of the SO and the outermost retinorecipient layers of the future SGFS. By ED12 the whole population of RGC have already enter the SO. Many SO axons branch and grow toward the TCC3, the inter TCC3-4 zone and the TCC4. The inter TCC3-4 zone thickens and the TCC3 and TCC4 are better defined. During DS7 the outermost TCC3 neurons acquire a horizontal orientation (Fig. 13). The TCC4 is mainly occupied by small neurons while the fibrous C "h" displays some scattered medium sized neurons (Fig. 12). The C "i-j" can now be separated into a neuronal C "i" and a fibrous C "j." The C "i" undergoes a decrease in thickness with respect to the precursor C "i-j." The immunochemical pattern of the C "i" however does not change significantly with respect to its precursor zone found at DS6. The fibrous C "j" appears as a dense network of neurites with a low density of small rounded neurons. The C "SGC" and C "SGP" immunolabeling resembles the pattern found at DS6 except for the Syt labeling which is now more neatly defined (Fig. 12). The C "SAC" remains almost unchanged. Figure 13 shows, at a higher magnification, the pattern of immunolabeling displayed by C "SGC," C "SAC," and "SGFP" during DS7. The PMZ disappears indicating that premigratory neurons are no longer present. However, some migrating neurons are still crossing the C "SAC." During DS7 the ex-GZ is invaded by some descending neurites (Fig. 12).

During DS7 the basic OT cortical organization is established. It displays the following radial organization: (1) the ex-GZ (future ependymal epithelium + sVZ), (2) the SGFP, (3) the C "SAC," (4) the C "SGC," (5) the C "j," (6) the C "i" and (7) the C "h" of the SGFS, (8) the TCC4 (precursor of layers "e" and "g" of the SGFS), (9) the inter TCC3-4 fibrous layer, (10) the TCC3 (precursor of layers "a" and "c" of the SGFS), and (11) the SO (Fig. 15). The post-DS7 phases of the OT corticogenesis were described previously (LaVail and Cowan, 1971a, 1971b; Scicolone et al., 1995).

Quantitative Data Associated to DSs Characterization

Records of NE cells proliferation. Figure 14 shows the statistical analysis of the NE cell proliferation data by DSs and EDs. The "*x-y*" plane, i.e., the DS-ED plane, represents a time-space window where the space axis is replaced by the spatial sequence of DS found along the developmental gradient axis at different EDs. The "*z*" axis corresponds to the values (mean ± standard deviation) of mitotic NE cells density. The shaded areas of the DS-ED plane indicate that each DS can be found at several EDs. Reciprocally, several DSs can be found at a particular ED. The grey ribbons within the cube depict the profiles of the mean values of mitotic NE cells density as a function of the DSs present at different EDs. The figure shows that the NE cell prolif-

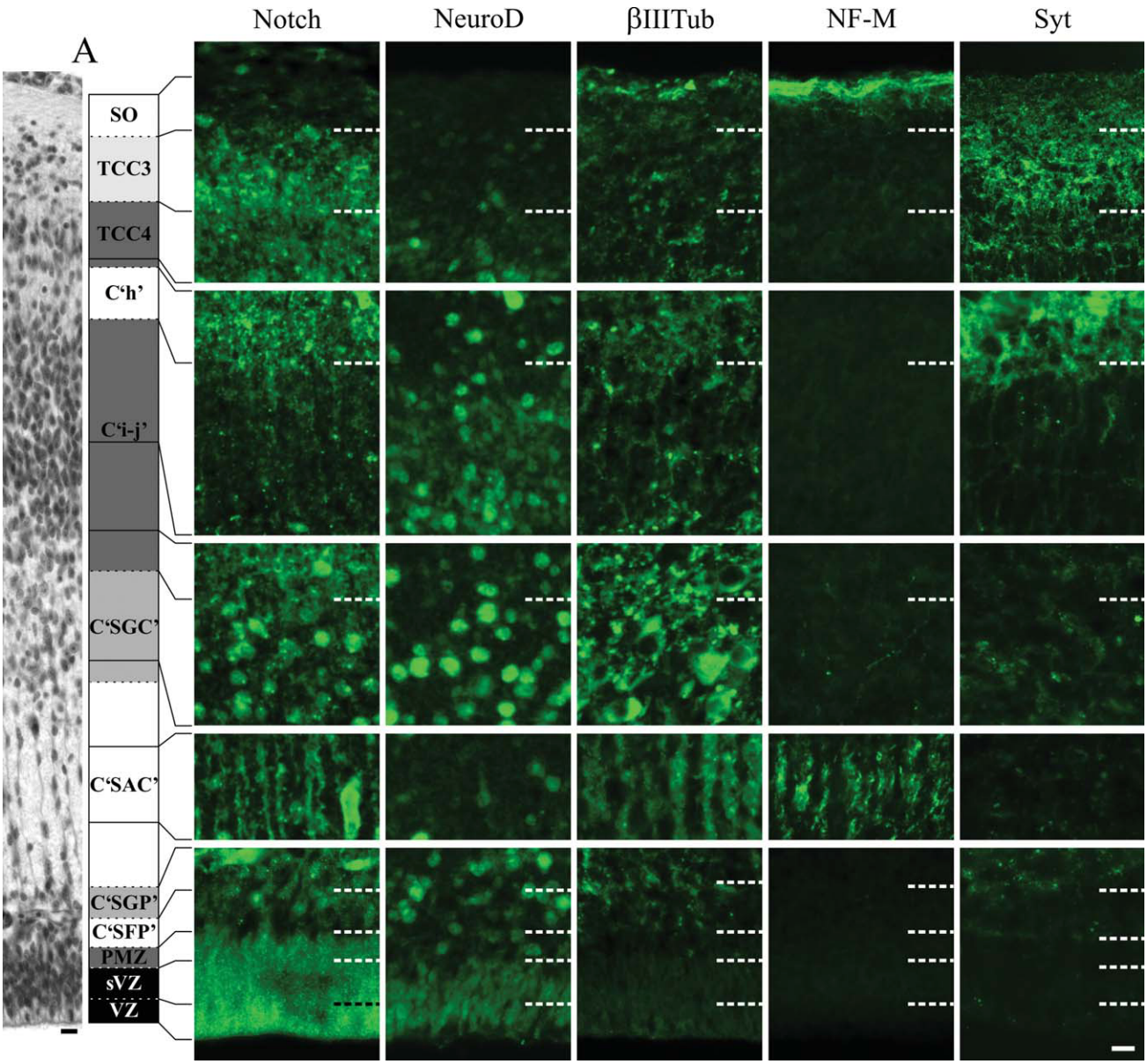

Fig. 10. Radial organization and immunocytochemical patterns during DS6 (ED10, HH36; ED12, HH38). The micrographs document the immunochemical pattern of each TCC (horizontally) and the radial pattern of expression of each antibody (vertically). (**A**) Hematoxylin-Eosin staining and schematic representation of the OT radial organization. Dotted lines indicate the limits between adjacent compartments. Full lines indicate the zone of each compartment corresponding to each horizontal series of micrographs. The TCC4 appears between the TCC3 and C "h." TCC3 and 4 are precursors of the retinorecipient layers. The SO displays intense NF-M and slight and irregular Syt and βIIITub labeling. The TCC3 neuropile and the C "h" (inter TCC4-2 fibrous layer) display intense Syt, Notch and βIIITub reactivity revealing intense neuritogenesis. The TCC4 neuropile shows a similar, although less intense, pattern. A few large slight NeuroD+ nuclei can be seen at the TCC3, TCC4 and C "h." The most superficial region of C "i-j," corresponding to about two-thirds of this compartment (bottom regions of the second row of immunohistochemical images), characterized by slightly Notch+ neuropile, a network of βIIITub+ and Syt+ neurites and NeuroD+ nuclei corresponds to the future C"i." The deeper third of C "i-j" (top region of the third row of immunohistochemical images) characterized by intense Notch+, βIIITub+ and slight Syt+ neuropile and low density of NeuroD+ nuclei corresponds to the future C "j." Large differentiating neurons with strong NeuroD+ nuclei are distributed along the radial axis, i.e., the C "SGC," C "SAC," C "SGP," and C "i-j". The largest neurons reside at the C "SGC" and also show βIIITub+ perikarya and Notch+ nuclei. With a less reactivity, the large C "SGP" neurons show a similar pattern. The C "SAC" displays the radial Notch+ NE cell basal processes and parallel βIIITub+ and NF-M+ axon fascicles; these axons no longer express Syt reactivity. A thin layer of slight Syt+ and βIIITub+ neurites (future C "SFP") appears below the C "SGP." The C "SFP" also displays a few large NeuroD+ nuclei. The cells of the ex GZ and the PMZ resume a strikingly intense Notch reactivity and display slight NeuroD+ nuclei. All these images correspond to sections along the cph-cd axis. Bars: 10 μm. [Color figure can be viewed in the online issue, which is available at wileyonlinelibrary.com.]

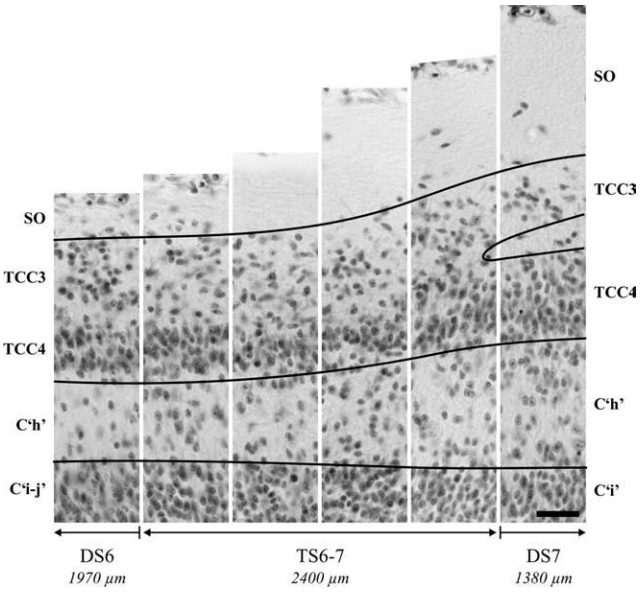

Fig. 11. Transitional changes between DS6 and DS7. The TS6-7 characteristics are documented by only four partial images of the transitional zone that covers a distance of around 2,400 μm of the section. The TS5-6 zone is "preceded" by a DS6 zone that linearly occupy around 2000 μm along the developmental gradient axis (on the left) and is "followed" by a DS7 zone that linearly occupy around 1400 μm length of the developmental gradient axis (on the right). These images where obtained from the same section shown in Fig. 9 and are a continuation of those images. Optic tectum (ED12, HH38) cut along the developmental gradient axis. Bar: 25 μm.

eration varies as a function of both the DS and the ED. The profile depicted on the "*x-z*" plane shows that the NE cell proliferation is DS-dependent. It shows a high proliferation during the early DSs (DS1-DS3) and then a gradual decrease followed by an abrupt decline from DS5 onwards. Afterwards, cell proliferation ceases. During DS1 and DS2 (ED2 to ED4) the OT is relatively small and the whole NE cell population shows a spatially homogeneous proliferation activity. However, from ED4 onwards, the DS-dependency is neatly revealed by the profiles depicted from ED6 to ED10.

The profile depicted on the "*y-z*" plane shows that the NE cell proliferation is ED-dependent. It shows a high increase in proliferation between ED2 and ED4 followed by a sustained decline in subsequent EDs and absence of proliferation at ED12. This profile reveals a developmentally regulated and ED-dependent NE cell proliferation.

Morphometric data: construction of a dynamic diagram of the OT corticogenesis. Morphometric data recorded at different DSs and EDs are presented in Supporting Information 2. The data illustrate the changes in thickness of the OT cortex and of each radial zone as a function of both the DS and the ED. They were used to build a 2D representation that dynamically illustrates the increase in complexity the OT cortex undergoes as a function of the DSs and the EDs (Fig. 15). This figure also shows that each ED corresponds to more than one DS and reciprocally.

3D Representation of the DSs Spatial Distribution as a Function of EDs

The 3D OT virtual images (Fig. 16) reveal that, at any ED, there is an ovoid-shaped ZMD located at the lateral region of the cephalic pole, i.e., the area of RGC axons ingression, and a thin crescent-shaped zone of minimal development bordering the caudal region of the OT dorsal midline. On each ED, several areas, corresponding to different DSs, are found as concentric bands around the ZMD (see Fig. 17). The 3D OT reconstructions show that each DS area travels as a propagating wave along the OT tangential plane as a function of the ED.

At the early stage (ED2/HH14) the entire OT surface is at the DS1. By ED4/HH23, the DS2 appears at the ZMD although no RGC axons can still be seen entering the OT. From ED4 onwards, each DS appears at the ZMD, travels through the lateral, dorsal and medial OT surfaces and disappears along the caudal dorsal midline (Fig. 16). See Supporting Information 3.

DS1–DS4 Areas Distribution on ED6

Between ED4 and ED6 there is a large tangential expansion of the OT wall accompanied by a rapid propagation of the DSs areas towards the caudal dorsal midline. Figure 16 (a) shows that the ZMD has reached the DS4 and is encircled by a TS3-4 band. The lateral view (b) shows that the TS3-4 band is followed by the DS3 one. The medial view (c) shows that the DS3 band is followed by a DS2 band and a thin DS1 band close to the caudal dorsal midline. The DS3, TS3-4, and DS4 bands are widely expanded over the lateral surface (a and b). Conversely, the DS2, DS3, and TS3-4 bands are "condensed" in the cephalic medial surface (c).

DS2–DS5 Areas Distribution on ED8

The frontal view (a) shows that the ZMD has reached the DS5 and is surrounded laterally by a TS4-5 band; this is, in turn, encircled by a DS4 band. The lateral view (b) shows that the TS3-4 band has moved over the OT lateral surface and has arrived near to the caudal pole. The medial view (c) shows that the DS3 band has moved to the medial surface and that the DS2 area is now restricted to a thin crescent-shaped area adjacent to the caudal region of the dorsal midline. The DS1 area has already disappeared. The medial view shows that the DSs are "condensed" between the ZMD and the anterior region of the dorsal midline.

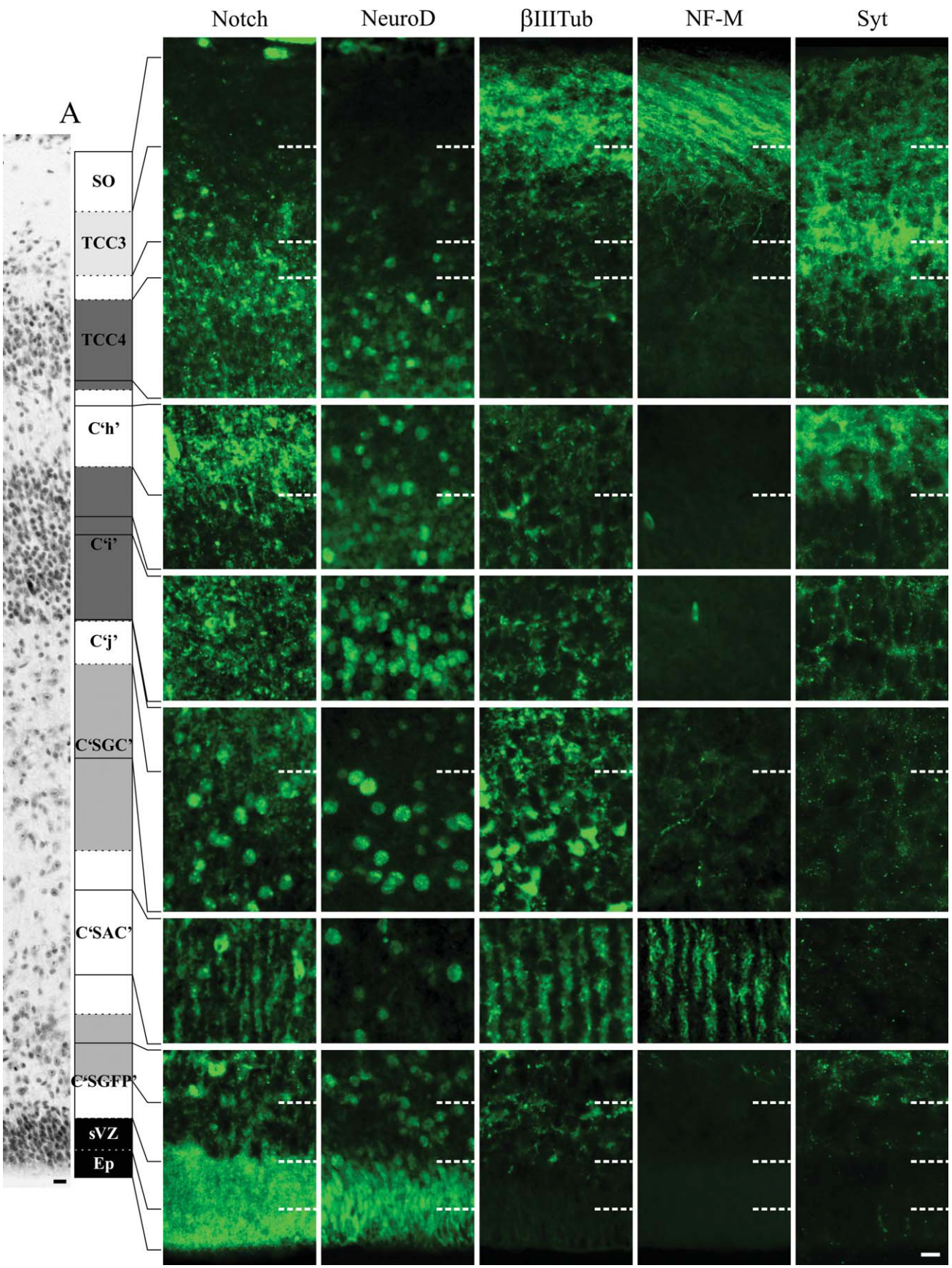
Notch
NeuroD
βIIITub
NF-M
Syt
A
SO
TCC3
TCC4
C'h'
C'i'
C'j'
C'SGC'
C'SAC'
C'SGFP'
sVZ
Ep

Fig. 12.

TS3-4 – TS6-7 Areas Distribution on ED10

Between ED8 and ED10 there is a rapid propagation of DSs from the ZMD towards the caudal dorsal midline. The ZMD has reached the TS6-7 which is surrounded by an extensive DS6 band (a). The TS5-6 has moved to the caudal lateral region and the caudal pole (b). The DS5 area has moved from the ZMD to the caudal pole. The caudal medial surface is now occupied by an extensive TS4-5 band, a small DS4 band and a crescent-shaped TS3-4 area near the caudal midline. DS3 and DS2 areas have disappeared. The DS6, TS5-6, DS5 and TS4-5 areas are "condensed" between the ZMD and the cephalic dorsal midline (c).

DS5–DS7 Areas Distribution on ED12

Between ED10 and ED12 the ZMD has progressed up to the DS7 (a); a fast propagation of the TS6-7 area towards the caudal pole, has also taken place (b). The medial aspect (c) is now occupied by the DS6 band surrounded by two semilunar areas, the TS5-6 and the DS5. The TS4-5, DS4 and TS3-4 areas have disappeared. The OT has underwent a large expansion forming a prominence between the lamina commissuralis and the tegmental region; thus, the ZMD is now almost completely encircled by the TS6-7, DS6 and TS5-6 areas [See views (c) and (a)].

DISCUSSION

The OT Development as a Temporal Sequence of DS. Temporal Organization of Developmental Cell Behaviors

By the end of its development, the OT is composed of alternating neuronal laminae and fibrous layers. The TCCs that emerge during the OT development are dynamic, self-organized neuronal associations with changing radial position and cell composition (Scicolone et al., 1995). Transient cell compartments are not precursors of particular definitive neuronal layers; they are composed of mixtures of neurons that will belong to different OT laminae. The structural changes and immunocytochemical patterns corresponding to the different DSs will be discussed in connection to several cell behaviors: neuroepithelial cells proliferation, neuronal migration, differentiation, neuritogenesis and synaptogenesis.

Neuroepithelial cell proliferation. It is intense during DS1-DS3, when the GZ is mainly occupied by Notch+ and Hes+ NE cell bodies. There is a period along which NE cells proliferation and Notch and Hes expressions overlap with neuronogenesis and neuronal migration. Both proteins are involved in expanding the NE cells pool by symmetric proliferation (Irvin et al., 2001; Akai et al., 2005; Basak and Taylor, 2007). Besides, Notch-Delta interactions regulate neuronogenesis (asymmetric NE cells proliferation, neuronal determination and differentiation) (Ma et al., 1996, 1998; Cisneros et al., 2008) and Hes expression is involved in NE cell maintenance and neuronogenesis (Nakazaki et al., 2008).

Neuronogenesis and early differentiation. The overlap between NE cells proliferation, neuronal determination and early differentiation coincides with the overlapped expressions of Notch, NeuroD, βIIITub and Syt. From DS1-DS2 onwards, NeuroD+ nuclei, indicative of neuronal commitment and/or differentiation (Katayama et al., 1997; Morrow et al., 1999; Cho and Tsai, 2004; Sanes et al., 2006), can be found intermingled with proliferating Notch+ NE cells. Expression of βIIITub identifies the earliest differentiating neurons, i.e., afferent (Mes5) and efferent (TCC1) neurons.

Three neuronogenic phases can be identified. The first one corresponds to the Mes5 neurons which are born along the dorsal midline during DS1 (ED2-ED4). The second one corresponds to the TCC1 neurons and the fast propagation of this TCC over the OT surface (DS2-DS3/ED4-ED6). These neurons first accumulate at the PMZ and begin the expression of βIIITub and Syt, indicating the onset of

Fig. 12. Radial organization and immunocytochemical patterns during DS7 (ED12, HH38). The micrographs document the immunochemical pattern of each TCC (horizontally) and the radial pattern of expression of each antibody (vertically). (**A**) Hematoxylin-Eosin staining and schematic representation of the OT radial organization. Dotted lines indicate the limits between adjacent compartments. Full lines indicate the zone of each compartment corresponding to the horizontal series of micrographs. The SO shows intense βIIITub+ and NF-M+ axons and irregular patches of slight Syt reactivity. The inter TCC3-4 fibrous zone and particularly the TCC3 neuropile show strongly Syt+ fibrous networks and a finely punctuate labeling. Except for a superficial band of the TCC3, the neuropile of the entire retinorecipient layers shows a punctuate pattern of Notch+ labeling. The future retinorecipient layers are invaded by NF-M+ and βIIITub+ SO axons branches. The TCC4 shows small NeuroD+ nuclei, some βIIITub+ perikarya and slightly Notch+, Syt+ and βIIITub+ neuropile. The fibrous C "h" shows intense Syt+ and Notch+ networks with a punctuate neuropile, a slight βIIITub+ neuropile and scattered medium sized NeuroD+ nuclei. The superficial zone of the C "i" shows medium-sized NeuroD+ nuclei with βIIITub+ perikarya and an irregular Notch+ and slight Syt+ neuropile labeling. The deep C "i" shows a high density of neurons with NeuroD+ nuclei and a neuropile with intensely Notch+ and βIIITub+ neurites and a punctuate Syt labeling. The C "j" shows a fibrous network of intense βIIITub+ neurites (axons), homogenous Notch+ neuropile, a low density of small NeuroD+ nuclei and some few oblique NF-M+ axons. The C "SGC," the C "SAC," the C "SGFP," although with a better defined pattern, display the characteristics of the DS6 (Compare with Fig. 10). The ex-GZ (sVZ + Ep) looks as a pseudostratified epithelium with intensely Notch+ cell bodies and intensely NeuroD+ nuclei. It is invaded by some descending neurites with a Syt+ bead-on-a-string labeling. All images correspond to cph-cd sections. Ep: ependymal epithelium. Bars: 10 μm. [Color figure can be viewed in the online issue, which is available at wileyonlinelibrary.com.]

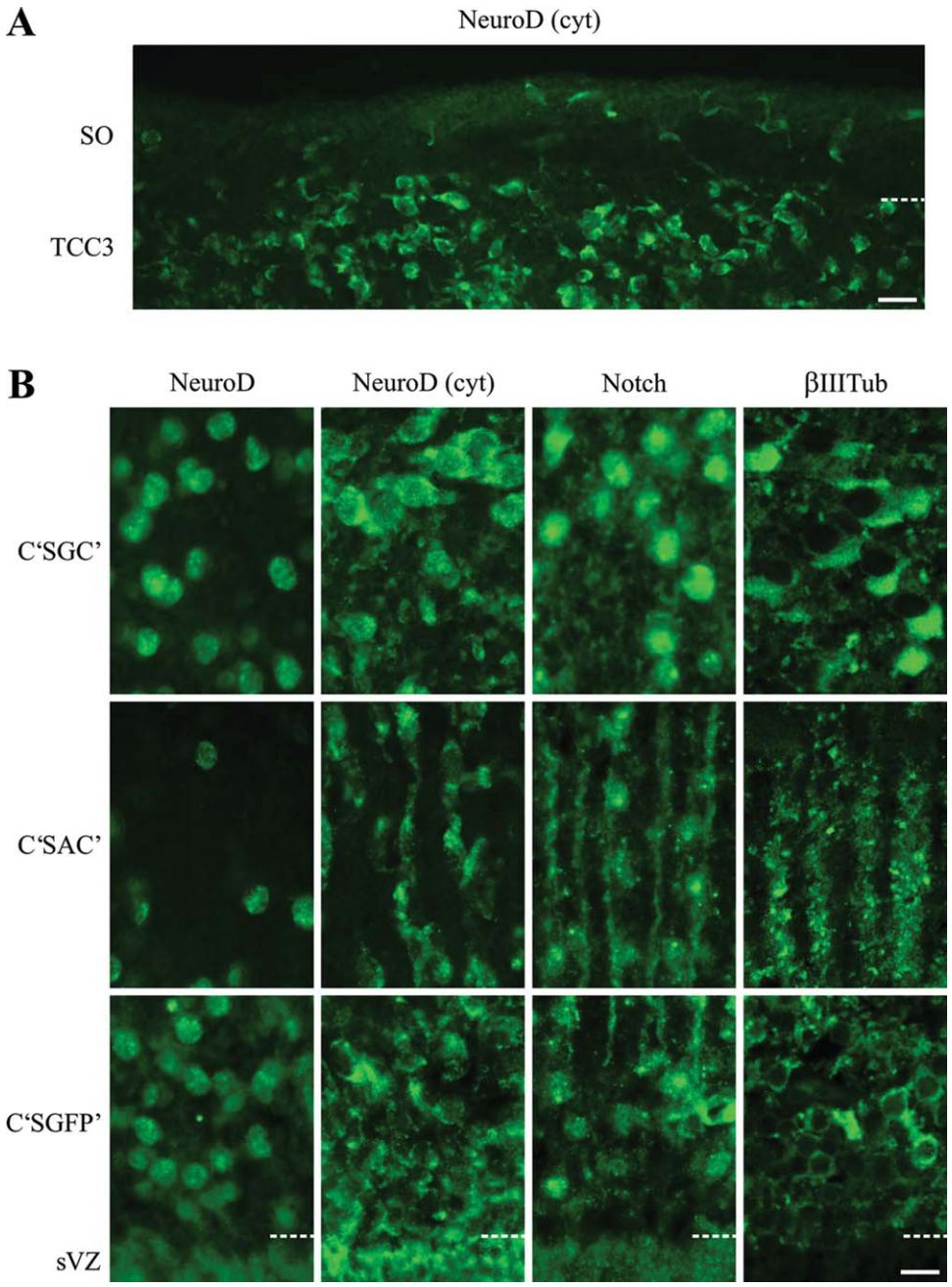

Fig. 13. (**A**) The NeuroD(cyt) staining shows that intrinsic neuritogenesis is taking place at the retinorecipient layers and that TCC3 neurons differentiate into polymorphic to horizontal small neurons. (**B**) Details of the NeuroD, Notch and βIIITub im muno-cytochemical pattern shown by the C "SGC," C "SAC," and C "SGFP." The NeuroD(cyt) labeling reveals that small fusiform radially oriented neurons (3rd neuronal cohort) can still be seen radially migrating across the C "SAC." Note that they reproduce the NE cells periodicity. This periodicity is also revealed by the distribution of the βIIITub+ tectal-bulbar tract axons. OT (ED12, HH38) cut along the developmental gradient axis. Bar: 10 μm. [Color figure can be viewed in the online issue, which is available at wileyonlinelibrary.com.]

somal differentiation and axonogenesis (Moody et al., 1989; Littleton et al., 1995; Haendel et al., 1996; Molea et al., 1999; Bergmann et al., 1999, 2000; Narayan and Greif, 2004). The earliest and the latest of these neurons will originate the SGC and the SGP neurons, respectively. The third phase corresponds to several subpopulations of small, radially oriented fusiform neurons (DS3-DS6/ED5.5-ED10) which will differentiate into the SGFS interneurons. They transiently accumulate at the PMZ and then migrate and stratify along the radial axis.

Neuronal migration and establishment of OT laminae. The Mes5 neurons first locate at the GZ-MZ interface. Most of them maintains that

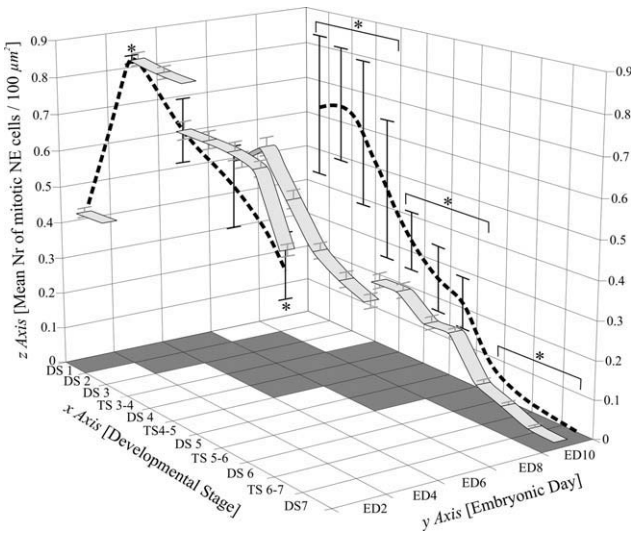

Fig. 14. 3D mesh graph of means values of mitotic NE cell density corresponding to the different DSs found along the developmental gradient axis at different EDs. The "*x-y*" plane, i.e., DS,ED plane, represents a time-space window because the series of DSs corresponds to sequences of segments of the developmental gradient axis. The values of the "*z*" axis within the "*x,y,z*" cube correspond to the mean ± standard deviation estimated for each DS at each ED [mean number of mitotic NE cells / 100 μm^2]. The grey ribbons represent the variations of this parameter as a function of the DSs recorded at different EDs. The small standard deviations of the mean values of these ribbons represent individual differences between homologous OT regions displaying the same DS and corresponding to the same ED. The values of the "*z*" axis represented on both the "*x-z*" and the "*y-z*" planes correspond to the mean ± standard deviation of the means values indicated within the cube. The large standard deviations observed on both planes derived from the fact they do not represent individual differences but results from the mixture of values corresponding to different EDs (*x-z* plane) or different DSs (*y-z* plane). Despite the large spread of values observed on the *x-z* and *y-z* planes, statistically significant differences were found within both planes. Three clusters of values -(DS1 – TS3-4), (DS4-DS5), (TS5-6 – DS7) with significant differences amongst them were found on the *x-z* plane ($p < 0.001$). Three clusters of values (ED2, ED6, ED8), (ED4), (ED10) with significant differences amongst them were found on the *y-z* plane ($p < 0.001$).

position at the GZ border and, by the final stages, resides near the SGFP. The remaining neurons emigrate to the mesenchymal tissue (Sánchez et al., 2002).

Transient cell compartment 1 neurons transiently aggregate at the PMZ (DS2 - TS3-4). During DS3–4, they leave the PMZ and differentiate into tangential fusiform neurons. The first of them will occupy the superficial SGC and presumably differentiate into type I SGC neurons; the following ones will form type II and III neurons (Luksch et al., 1998; Wu et al., 2000; Heidmann and Luksch, 2001; Luksch 2003). The last neurons to leave the PMZ lay at the deep TCC1 and will reside at the SGP. Between DS3–TS4-5, they form a narrow TCC1. During DS5, the TCC1 neurons axons form the C "SAC" and the TCC1 neurons are thus segregated into two subpopulations: the C "SGC" and the C "SGP."

During the TCC1 formation, the PMZ is occupied by the future SGFS interneurons. By DS3 - TS3-4, the outermost of these neurons migrate radially along the NE cells basal processes, as it has been reported in many CNS areas (Rakic, 1972; Rakic et al., 1994; Anton et al., 1996). Their ordered migration results in an inside-out pattern, partially resembling that found in the brain cortex (Campbell, 2005; Kriegstein et al., 2006; Rakic, 2006). Beyond the TCC1, these neurons form the TCC2 (DS4). Between TS4-5 and DS5, the TCC2 increases in thickness. During DS5 a subpopulation of neurons surpasses the TCC2, originating the TCC3. During DS6, a sorting-out of the remaining TCC2 neurons originates the TCC4 and the C "i-j." This stratification is accompanied by the appearance of fibrous layers delimiting adjacent TCCs. Regarding the post-DS7 (ED12/HH38), previous papers have already reported, using a different nomenclature, that the TCC3 segregates into layers "a" and "c" of the SGFS, while the TCC4 delaminates into layers "e" and "g" (LaVail and Cowan, 1971a; Scicolone et al., 1995). In turn, the C "i-j" neurons spread along the radial axis and form layers "h", "i", and "j" of the SGFS. Most of the SGFS neurons begin βIIITub expression after arriving at their postmigratory positions.

Axono-, dendrito- and synaptogenesis. Optic nerve axons enter the OT cephalic pole by ED6 (LaVail and Cowan, 1971a; Thanos and Bonhoeffer, 1987). The firsts of them proceed from retinal area centralis (Thanos and Mey, 2001). During DS6, the SO thickens by a massive ingression of βIIITub+ and NF-M+ axons. During DS7, the SO axons profusely ramify but their growth is limited to the TCC3 and the inter TCC3-4 layer revealing that the boundary between retinorecipient and nonretinorecipient laminae (Seo et al., 2008; Jiang et al., 2009) are already established.

Large afferent (Mes5) and efferent (TCC1) neurons begin neuritogenesis earlier than the SGFS interneurons. During DS1, the Mes5 neurons originate a βIIITub+, Syt+ and NF-M+ neurite and transform into pseudounipolar neurons whose axons follow a dorsal-ventral direction. During DS2, the TCC1 neurons originate axons that are guided to grow in a dorsal-ventral direction (Islam et al., 2009; Naser et al., 2009). During DS2, axons from the TCC1 and Mes5 neurons run superficially. From DS5 onwards, they form the C "SAC" after the inside-out migration of SGFS interneurons. By DS5 the C "SGC" neurons initiate a second phase of cytoplasmic Notch expression and, by DS6, they transform into large multipolar neurons with intense Notch nuclear labeling. These changes are suggestive of dendritogenesis since Notch signaling regulates dendrite length and branching pattern (Sestan et al., 1999; Redmond et al., 2000, Red-

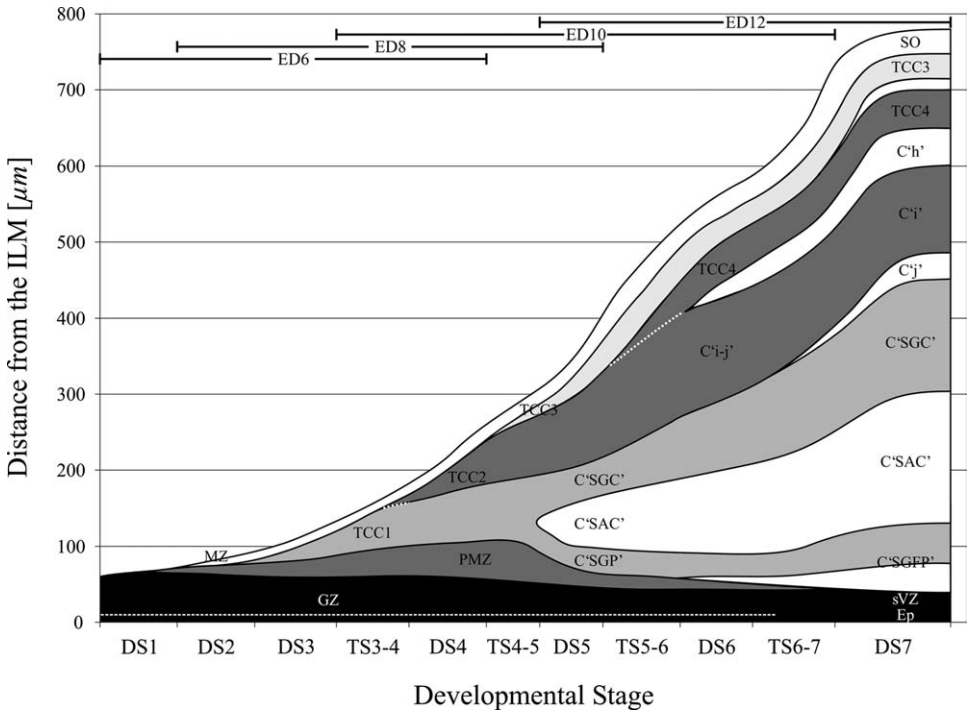

Fig. 15. DSs and EDs are represented on the *x* axis. The thickness [μm] of every radial zone and of the entire OT wall (distance between the ILM and OLM) is indicated on the *y* axis. This schematic representation of the changes in the OT organization as a function of the DSs dynamically illustrates the tectal corticogenesis and shows that several spatially organized areas corresponding to increasing DSs can be found at each ED. This explains why EDs overlap over the *x* axis.

mond and Ghosh, 2001; Whitford et al., 2002). By DS6 a pattern of βIIITub, Syt and Notch reactivity, which is commonly associated to neuritogenesis (Basarsky et al., 1994; Redmond et al., 2000) become ostensible at TCC3 neuropile. This neuropile will contribute to the adult layer "c" corresponding to the zone of terminal dendritic branches of the type III SGC neurons. Simultaneously, the C "h" (future adult layer "h") which corresponds to the terminal dendrites of the type II SGC neurons exhibits the same immunochemical pattern. Between DS6–7 these layers remarkably increase in thickness and by DS7 a new fibrous band, the inter TCC3-4 (the future adult layer "d"), corresponding to the zone of endings of the dendritic tree of the type I SGC neurons displays the typical pattern of dendritogenesis. All these fibrous layers are not only populated by dendritic branches from the SGC but also by a variety of neurites originated by the SGFS local interneurons (Deng and Rogers, 1998; Wu et al., 2000; Heidmann and Luksch, 2001; Luksch 2003; Yamagata et al., 2006). The C "SGP" neurons display a similar immunolabeling but a lesser reactivity than "SGC" neurons.

During DS7 a new Notch+, βIIITub+ and Syt+ fibrous band, the C "j," appears between the ex-TCC2, i.e., the C "i," and the C "SGC"; the C "SFP" also displays Notch, βIIITub and Syt reactivity. During DS7 the future retinorecipient layers, i.e., the TCC3 and the inter TCC3-4, and the C "h" develop a punctuate pattern of Notch and Syt labelling. Sparser Syt labelling is also observed around the C "i" neurons, at the C "j" neuropile, and around the C "SGC" and C "SGFP" neurons. Significantly, Notch signaling plays a role in the regulation of axono- and dendritogenesis (Giniger, 1998; Whitford et al., 2002) and a punctuate pattern of Syt labeling characterizes synaptogenesis (Littleton et al., 1993; Basarsky et al., 1994; Dubuque et al., 2001). The large and medium-sized neurons scattered along the entire radial axis also display Notch+ and NeuroD+ nuclei during this neuritogenic phase.

Considerations about gliogenesis. By DS5 the NE cells proliferation and the Notch reactivity decline at the GZ. By DS6-DS7 the proliferation activity has completely ceased but the Notch reactivity and the NeuroD nuclear labeling are resumed. Notch and NeuroD signaling play a role in the process of neuronal vs. glial determination (Inoue et al., 2002) and the chronology and the spatial organization of the OT gliogenesis (Galileo, 2003; Kim et al., 2006; Seo et al., 2008) suggest that the pattern of immunolabeling observed at the ex-GZ by DS6-7 may be associated to gliogenesis.

Spatial propagation of DSs as a function of the ED. The description of a developing system in terms of a temporal sequence of DSs fails to capture the spatial complexity when spatially asymmetric systems are considered (Poole, 1988; Bege-

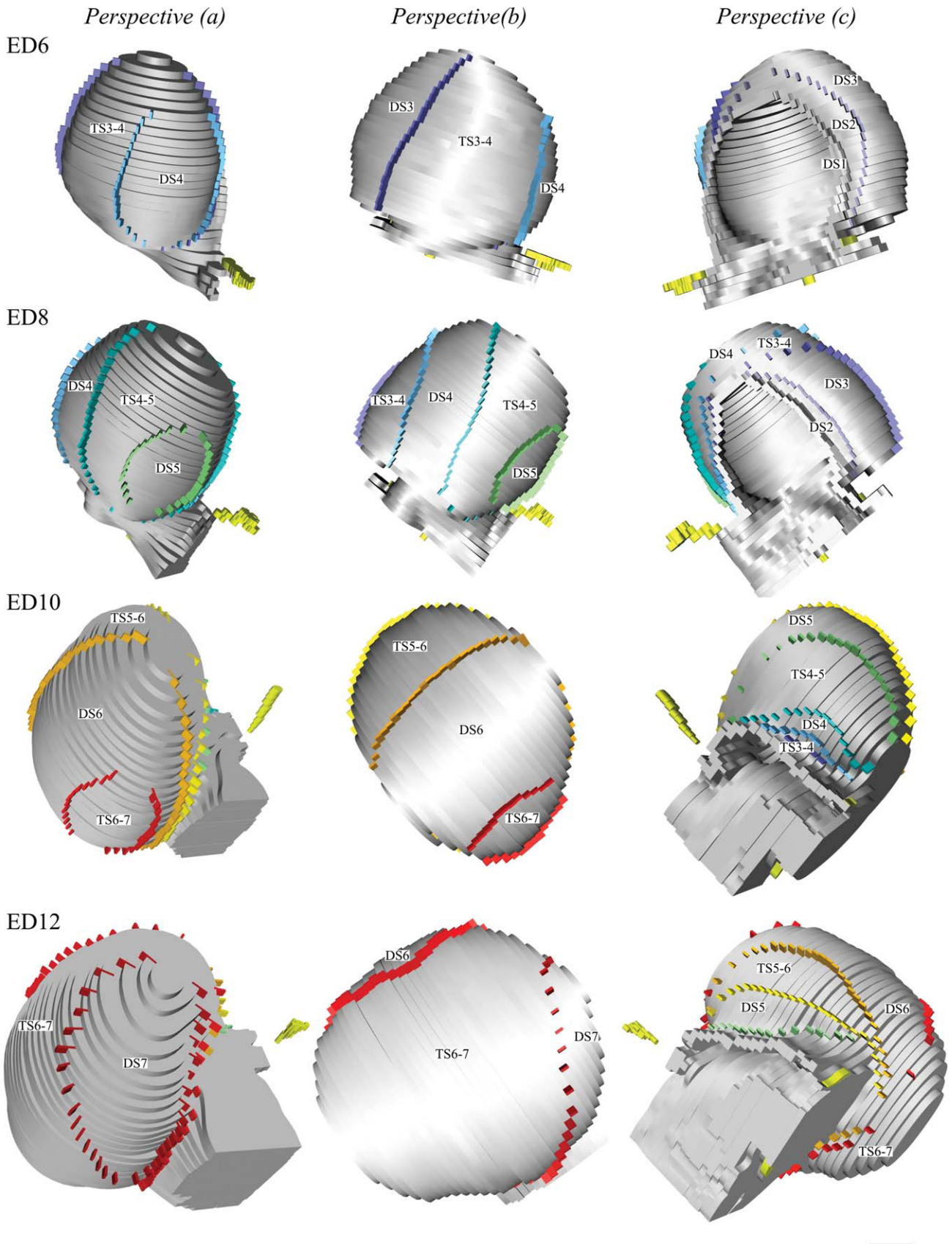

Fig. 16. Spatial propagation of DSs areas as a function of the ED. Three different aspects (a, b, and c) of the same 3D virtual image are shown for each ED. The three perspectives reveal how the DSs areas propagate from the cephalic pole to the caudal dorsal midline. The three views correspond to: (**A**) A front and top view of the cephalic pole allows seeing the position of the zone of maximal development (ZMD) and of the neighboring DSs areas; (**B**) A right lateral view allows seeing the DSs areas propagating towards the caudal pole; (**C**) A medial view shows how the DSs areas distribute over the medial surface towards the caudal region of the dorsal midline (zone of minimal development). The OT cephalic pole is on the right in (b) and on the left in (c). The position of three medial elements, (1) the pineal gland; (2) the emergence of the III cranial nerve; and (3) the IV cranial nerve decussation are marked (dark gray) as topographical references. See Supporting Information 3: 3D Animation showing a 360° rotation of the 3D OT virtual images. Bar: 500 μm. [Color figure can be viewed in the online issue, which is available at wileyonlinelibrary.com.]

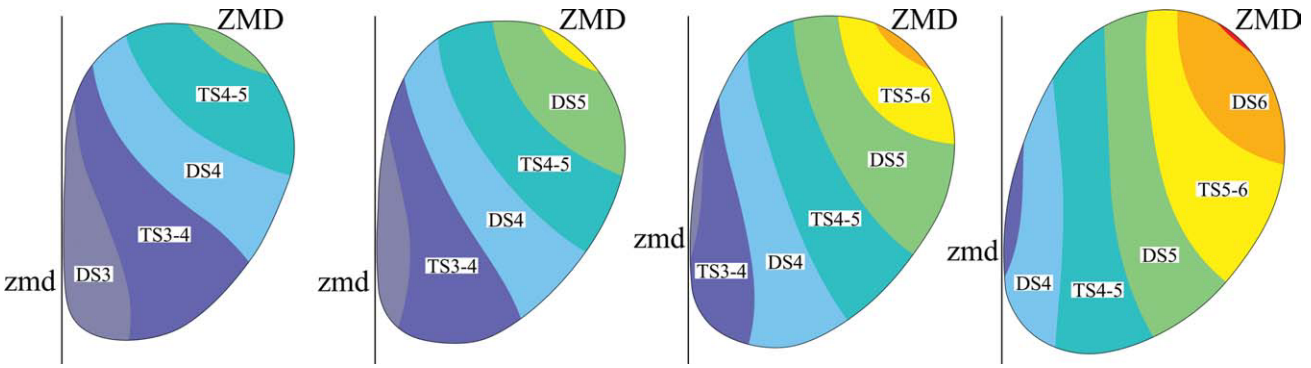

Fig. 17. Schematic 2D representation illustrating the spatial propagation of areas corresponding to different DSs along the developmental gradient axis. The series illustrates that each DS appears at the zone of maximal development (ZMD) on the lateral aspect of the cephalic pole and from this zone propagates as a migrating wave towards the zone of minimal development (zmd) located at the caudal region of the dorsal midline. See Supporting Information 4: 2D Animation of DSs areas propagation over the OT tangential plane. [Color figure can be viewed in the online issue, which is available at wileyonlinelibrary.com.]

mann and Meyer, 2001; Dubrulle et al., 2001; Bel-Vialar et al., 2002; Drawbridge et al., 2003; Andrade et al., 2005; Trainor, 2005; Rochais et al., 2009; van den Berg et al., 2009). The present paper introduces a table of DSs of the OT development that dynamically observe the following facts: (a) several spatially organized DSs are simultaneously present at any ED or HH stage; (b) DSs progress as a function of the time; (c) DSs areas move along the cph-cd axis; (d) DSs overlap in the temporal domain, but can be distinctly resolved in the spatial domain; (e) the inclusion of TSs between temporally subsequent/spatially adjacent DSs observe the continuity of the developing changes; and (f) every DS first appears at the site where the optic nerve axons enter the OT, propagates over the tectal wall and eventually disappears at the caudal region of the dorsal midline. Figure 17 shows a simplified example of the DSs areas propagation (See Supporting Information 4). The area occupied by each DS on subsequent EDs depends on the DS duration; i.e., the longer the DS duration, the larger its corresponding area.

The existence of several different DSs along the cph-cd axis introduces position-dependent differences even in biochemical assays in which spatial specifications seem to be unimportant. As an example, the value of uPA activity, i.e., an enzyme involved in neuronal migration (Friedman and Seeds, 1995; Barber et al., 2008), measured in soluble fractions of entire OTs (Pereyra-Alfonso et al., 1994) significantly differs from the enzyme activity assayed in soluble fractions of either cephalic or caudal halves (Pereyra-Alfonso et al., 1998). Disregarding the spatial asymmetry leads to biochemical results that do not correspond to any OT region or any DS.

The progression of the OT development expressed as sequences of DSs along the developmental gradient axis. The table of DSs introduced in this paper can be advantageously used to characterize histological sections of the OT as well as to characterize the OT global development. The presence of several DSs at any ED or HH stage indicates that histological preparations (immunocytochemistry, in situ hybridization, etc.) of the developing OT cannot be reliably characterized by simply specifying the ED or the HH stage. A reliable interpretation of such preparations requires the specification of at least five parameters: (a, b) the ED and HH stage; (c) the DS of the illustrated region; (d) the plane of section orientation (e.g., d-v section); and (e) the position of the section with respect to another orthogonal axis, i.e., d-v section located at a particular position along the cph-cd axis. Given that many researchers have adopted the convention to display d-v sections located half way between the OT cephalic and caudal poles, in these cases, two specifications (the HH embryonic stage + the OT DS) are enough to give an identity to the section and to make appropriate comparisons between different specimens. However, any attempt to globally characterize the OT development requires an examination along the entire developmental gradient axis. In these cases, sections coinciding with the developmental gradient axis orientation should be preferred. Only sections with this orientation allow characterizing the global OT developmental progression in terms of complete sequences of DSs along the developmental gradient axis.

ACKNOWLEDGMENTS

The monoclonal antibody 4H6 (antineurofilament) developed by Willi Halfter was obtained from the Developmental Studies Hybridoma Bank developed under the auspices of the NICHD and maintained by The University of Iowa, Department of Biological Sciences, Iowa City, IA 52242.

LITERATURE CITED

Akai J, Halley PA, Storey KG. 2005. FGF-dependent Notch signaling maintains the spinal cord stem zone. Genes Dev 19:2877–2887.

Andrade RP, Pascoal S, Palmeirim I. 2005. Thinking clockwise. Brain Res Rev 49:114–119.

Anton ES, Cameron RS and Rakic P. 1996. Role of neuron-glial junctional domain proteins in the maintenance and termination of neuronal migration across the embryonic cerebral wall. J Neurosci 16:2283–2293.

Barber M, Lino N, Rapacioli M, Teruel L, Di Nápoli J, Rodríguez Celín A, Duarte S, Sánchez V. 2008. The uPA-PAI1-uPAR complex promotes neuronal migration and neuritogenesis in vitro. In: Proceedings of the 4th International Meeting of the Latin American Society for Developmental Biology (LASDB). Buenos Aires, Argentina. November 1–3.

Basak O, Taylor V. 2007. Identification of self-replicating multipotent progenitors in the embryonic nervous system by high Notch activity and Hes5 expression. Eur J Neurosci 25:1006–1022.

Basarsky TA, Parpura V and Haydon PG. 1994. Hippocampal synaptogenesis in cell culture: Developmental time course of synapse formation, calcium influx, and synaptic protein distribution. J Neurosci 14:6402–6411.

Begemann G, Meyer A. 2001. Hindbrain patterning revisited: Timing and effects of retinoic acid signalling. Bioessays 23:981–986.

Bel-Vialar S, Itasaki N, Krumlauf R. 2002. Initiating Hox gene expression: In the early chick neural tube differential sensitivity to FGF and RA signaling subdivides the HoxB genes in two distinct groups. Development 129:5103–515.

Bergmann M, Grabs D, Rager G. 1999. Developmental expression of dynamin in the chick retinotectal system. J Histochem Cytochem 47:1297–1306.

Bergmann M, Grabs D, Rager G. 2000. Expression of presynaptic proteins is closely correlated with the chronotopic pattern of axons in the retinotectal system of the chick. J Comp Neurol 418:361–372.

Campbell K. 2005. Cortical neuron specification: It has its time and place. Neuron 46:373–376.

Cho JH, Tsai MJ. 2004. The role of BETA2/NeuroD1 in the development of the nervous system. Mol Neurobiol 30:35–47.

Cisneros E, Latasa MJ, García-Flores M, Frade JM. 2008. Instability of Notch1 and Delta1 mRNAs and reduced Notch activity in vertebrate neuroepithelial cells undergoing S-phase. Mol Cell Neurosci 37:820–831.

Coggeshall RE and Lekan HA. 1996. Methods for determining numbers of cells and synapses: A case for more uniform standards of review. J Comp Neurol 364:6–15.

Deng C, Rogers LJ. 1998. Organisation of the tectorotundal and SP/IPS-rotundal projections in the chick. J Comp Neurol 394:171–85.

Drawbridge J, Meighan CM, Lumpkins R, Kite ME. 2003. Pronephric duct extension in amphibian embryos: Migration and other mechanisms. Dev Dyn 226:1–11.

Dubrulle J, McGrew MJ, Pourquié O. 2001. FGF signaling controls somite boundary position and regulates segmentation clock control of spatiotemporal Hox gene activation. Cell 106:219–232.

Dubuque SH, Schachtner J, Nighorn AJ, Menon KP, Zinn K, Tolbert LP. 2001. Immunolocalization of synaptotagmin for the study of synapses in the developing antennal lobe of Manduca sexta. J Comp Neurol 441:277–287.

Eyal-Giladi H, Kochav S. 1976. From cleavage to primitive streak formation: A complementary normal table and a new look at the first stages of the development of the chick. I. Gen Morphol Dev Biol 49:321–337.

Firka D, Rapacioli M, Fuentes F, Ortalli A, Sanchez V, Scicolone G, D'atellis CE, Flores V. 2004. Designing a computer software program for complex border detection. Biological application. WSEAS Trans Biol Biomed 1:24–30.

Friedman GC, Seeds NW. 1995. Tissue plasminogen activator mRNA expression in granule neurons coincides with their migration in the developing cerebellum. J Comp Neurol 360:658–670.

Fujita S. 1964. Analysis of neuron differentiation in the central nervous system by tritiated thymidine autoradiography. J Comp Neurol 122:311–328.

Fujita S. 1967. Application of light and electron microscopic autoradiography to the study of cytogenesis of the forebrain. In: Hassler R, Stephan H, editors. The Evolution of Forebrain. New York: Plenum. pp 180–196.

Fujita S. 1997. Cell differentiation and ontogeny of the nervous system. In: Dani SU, Hori A, Walter G, editors. Neural ageing. Amsterdam, NL: Elsevier. pp 129–151.

Fujita S. 2003. The discovery of the matrix cell, the identification of the multipotent neural stem cell and the development of the central nervous system. Cell Struct Funct 28:205–228.

Galileo DS. 2003. Spatiotemporal gradient of oligodendrocyte differentiation in chick optic tectum requires brain integrity and cell-cell interactions. Glia 41:25–37.

Giniger E. 1998. A role for Abl in notch signaling. Neuron 20:667–681.

González MA, Rapacioli M, Ballarín VL, Fiszer de Plazas S, Flores V. 2007. Digital processing of in situ hybridization images: Identification and spatial allocation of specific labels. J Comp Sci Tech 7:243–248.

Haendel MA, Bollinger KE, Baas PW. 1996. Cytoskeletal changes during neurogenesis in cultures of avian neural crest cells. J Neurocytol 25:289–301.

Hamburger V, Hamilton H. 1951. A series of normal stages in the development of the chick embryo. J Morphol 88:48–92.

Heidmann S, Luksch H. 2001. Development of retino-recipient projection neurons in the optic tectum of the chicken. Brain Res Dev Brain Res 128:149–156.

Hopwood N. 2007. A history of normal plates, tables and stages in vertebrate embryology. Int J Dev Biol 51:1–26.

Inoue T, Hojo M, Bessho Y, Tano Y, Lee JE, Kageyama R. 2002. Math3 and NeuroD regulate amacrine cell fate specification in the retina. Development 129:831–842.

Irvin DK, Zurcher SD, Nguyen T, Weinmaster G, Kornblum HI. 2001. Expression patterns of Notch1, Notch2, and Notch3 suggest multiple functional roles for the Notch-DSL signaling system during brain development. J Comp Neurol 436:167–181.

Islam SM, Shinmyo Y, Okafuji T, Su Y, Naser IB, Ahmed G, Zhang S, Chen S, Ohta K, Kiyonari H, Abe T, Tanaka S, Nishinakamura R, Terashima T, Kitamura T, Tanaka H. 2009. Draxin, a repulsive guidance protein for spinal cord and forebrain commissures. Science 323:388–393.

Itasaki N, Ichijo H, Hama C, Matsuno T and Nakamura H. 1991. Establishment of rostrocaudal polarity in tectal primordium: Engrailed expression and subsequent tectal polarity. Development 113:1133–1144.

Jiang YQ, Oblinger MM. 1992. Differential regulation of beta III and other tubulin genes during peripheral and central neuron development. J Cell Sci 103(Part3):643–651.

Jiang Y, Obama H, Kuan SL, Nakamura R, Nakamoto C, Ouyang Z, Nakamoto M. 2009. In vitro guidance of retinal axons by a tectal lamina-specific glycoprotein Nel. Mol Cell Neurosci 41:113–119.

Johnson GV, Jope RS. 1992. The role of microtubule-associated protein 2 (MAP-2) in neuronal growth, plasticity, and degeneration. J Neurosci Res 33:505–512.

Kabayama H, Takei K, Fukuda M, Ibata K, Mikoshiba K. 1999. Functional involvement of synaptotagmin I/II C2A domain in neurite outgrowth of chick dorsal root ganglion neuron. Neuroscience 88:999–1003.

Katayama M, Mizuta I, Sakoyama Y, Kohyama-Koganeya A, Akagawa K, Uyemura K, Ishii K. 1997. Differential expression of neuroD in primary cultures of cerebral cortical neurons. Exp Cell Res 236:412–417.

Kim DW, Park SW, Jeon GS, Seo JH, Golden JA, Cho SS. 2006. The multiple dorsoventral origins and migratory pathway of

tectal oligodendrocytes in the developing chick. Brain Res 1076:16–24.
Kriegstein A, Noctor S, Martínez-Cerdeño V. 2006. Patterns of neural stem and progenitor cell division may underlie evolutionary cortical expansion. Nat Rev Neurosci 7:883–890.
Lai EC. 2004. Notch signaling: Control of cell communication and cell fate. Development 131:965–973.
Lalonde R, Strazielle C. 2003. Neurobehavioral characteristics of mice with modified intermediate filament genes. Rev Neurosci 14:369–385.
LaVail JH, Cowan WM. 1971a. The development of the chick optic tectum. I. Normal morphology and cytoarchitectonic development. Brain Res 28:391–419.
LaVail JH, Cowan WM. 1971b. The development of the chick optic tectum. II. Autoradiographic studies. Brain Res 28:421–441.
Lee MK, Tuttle JB, Rebhun LI, Cleveland DW, Frankfurter A. 1990. The expression and posttranslational modification of a neuron-specific beta-tubulin isotype during chick embryogenesis. Cell Motil Cytoskeleton 17:118–132.
Littleton JT, Bellen HJ, Perin MS. 1993. Expression of synaptotagmin in *Drosophila* reveals transport and localization of synaptic vesicles to the synapse. Development 118:1077–1088.
Littleton JT, Upton L, Kania A. 1995. Immunocytochemical analysis of axonal outgrowth in synaptotagmin mutations. J Neurochem 65:32–40.
Lou X, Bixby JL. 1993. Coordinate and noncoordinate regulation of synaptic vesicle protein genes during embryonic development. Dev Biol 159:327–337.
Luksch H. 2003. Cytoarchitecture of the avian optic tectum: Neuronal substrate for cellular computation. Rev Neurosci 14:85–106.
Luksch H, Cox K and Karten HJ. 1998. Bottlebrush dendritic endings and large dendritic fields: Motion-detecting neurons in the tectofugal pathway. J Comp Neurol 396:399–414.
Ma Q, Kintner C, Anderson DJ. 1996. Identification of neurogenin, a vertebrate neuronal determination gene. Cell 87:43–52.
Ma Q, Chen Z, del Barco Barrantes I, de la Pompa JL, Anderson DJ. 1998. neurogenin1 is essential for the determination of neuronal precursors for proximal cranial sensory ganglia. Neuron 20:469–482.
Matus A. 1990. Microtubule-associated proteins and the determination of neuronal form. J Physiol 84:134–137.
Matsuno T, Ichijo H and Nakamura H. 1991. Regulation of the rostrocaudal axis of the optic tectum: Histological study after rostrocaudal rotation in quail-chick chimeras. Dev Brain Res 58:265–270.
Mazzeo J, Rapacioli M, Fuentes F, Di Guilmi M, Ortalli A, D'Attellis CE, Flores V. 2004. Space sequences reveal an organized neuroepithelial cell proliferation in the developing central nervous system. WSEAS Trans Biol Biomed 4:441–448.
Mey J, Thanos S. 2000. Development of the visual system of the chick. I. Cell differentiation and histogenesis. Brain Res Brain Res Rev 32:343–379.
Molea D, Stone JS, Rubel EW. 1999. Class III beta-tubulin expression in sensory and nonsensory regions of the developing avian inner ear. J Comp Neurol 406:183–198.
Moody SA, Quigg MS, Frankfurter A. 1989. Development of the peripheral trigeminal system in the chick revealed by an isotype-specific anti-beta-tubulin monoclonal antibody. J Comp Neurol 279:567–580.
Morrow EM, Furukawa T, Lee JE, Cepko CL. 1999. NeuroD regulates multiple functions in the developing neural retina in rodent. Development 126:23–36.
Nakazaki H, Reddy AC, Mania-Farnell BL, Shen YW, Ichi S, McCabe C, George D, McLone DG, Tomita T, Mayanil CS. 2008. Key basic helix-loop-helix transcription factor genes Hes1 and Ngn2 are regulated by Pax3 during mouse embryonic development. Dev Biol 316:510–523.
Narayan S, Greif KF. 2004. Transport of a synaptotagmin-YFP fusion protein in sympathetic neurons during early neurite outgrowth in vitro after transfection in vivo. J Neurosci Methods 133:91–98.
Naser IB, Su Y, Islam SM, Shinmyo Y, Zhang S, Ahmed G, Chen S, Tanaka H. 2009. Analysis of a repulsive axon guidance molecule, draxin, on ventrally directed axon projection in chick early embryonic midbrain. Dev Biol 332:351–359.
O'Rahilly R, Muller F. 1987. Developmental Stages in Human Embryos: Including a Revision of Streeter's "Horizons" and a Survey of the Carnegie Collection. Washington DC: Carnegie Institution of Washington. p N 637.
Pereyra-Alfonso S, Scicolone G, Fiszer De Plazas S, Pecci Saavedra J, Flores V. 1994. Current Triton X-100 treatments do not allow a complete plasminogen activator extraction from developing nervous tissue. Neurochem Res 20:137–142.
Pereyra-Alfonso S, Sanchez V, Scicolone G, Ferrán JL, Flores V. 1998. Cephalo-caudal gradient of plasminogen activator expression in the developing chick optic lobe. In: Proceedings of the 5th Brazilian Symposium on Extracellular Matrix SIMEC 98, Angra dos Reis. Brasil. September 7–10.
Perrot R, Berges R, Bocquet A, Eyer J. 2008. Review of the multiple aspects of neurofilament functions, and their possible contribution to neurodegeneration. Mol Neurobiol 38:27–65.
Poole TJ. 1988. Cell rearrangement and directional migration in pronephric duct development. Scanning Microsc 2:411–415.
Puelles L, Bendala MC. 1978. Differentiation of neuroblasts in the chick optic tectum up to eight days of incubation: A Golgi study. Neurosci 3:307–325.
Rakic P. 1972. Mode of cell migration to the superficial layers of fetal monkey neocortex. J Comp Neurol 145:61–83.
Rakic P, Cameron RS, Komuro H. 1994. Recognition, adhesion, transmembrane signaling and cell motility in guided neuronal migration. Curr Opin Neurobiol 4:63–69.
Rakic P. 2006. A century of progress in corticoneurogenesis: From silver impregnation to genetic engineering. Cereb Cortex 16(Suppl 1):i3–i17.
Rapacioli M, Gigola S, D'Attellis CE, Ferrán JL, Pereyra-Alfonso S, Sánchez V and Flores V. 2000. Analysis of cell proliferation as stochastic point process. In: Mastorakis NE, editor. Mathematics and Computers in Modern Science. New York: World Scientific and Engineering Society Press. pp 23–28.
Rapacioli M, Gigola S, D'Attellis CE, Ferrán JL, Pereyra-Alfonso S, Sanchez V, Scicolone G, Flores V. 2001a. Definition of developmental locus property in terms of space-dependent changes in dynamics of developmental mechanisms: The postmitotic neuronal migration in the developmental central nervous system. In: Mastorakis NE, editor. Mathematics and simulation with biological applications. New York: World Scientific and Engineering Society Press. pp 196–201.
Rapacioli M, D'Attellis C, DiMiro A, Spraggon T, Ferrán JL, Pereyra Alfonso S, Sanchez V, Scicolone G, Flores V. 2001b. Attempts to mathematically define a developmental gradient. The isthmic organizer and the postmitotic neuronal migration dynamics in the developing central nervous system. In: Mastorakis NE, editor. Mathematics and simulation with biological applications. New York: World Scientific and Engineering Society Press. pp 137–142.
Redmond L, Oh SR, Hicks C, Weinmaster G, Ghosh A. 2000. Nuclear Notch1 signaling and the regulation of dendritic development. Nat Neurosci 3:30–40.
Redmond L, Ghosh A. 2001. The role of notch and Rho GTPase signaling in the control of dendritic development. Curr Opin Neurobiol 11:111–117.
Rochais F, Mesbah K, Kelly RG. 2009. Signaling pathways controlling second heart field development. Circ Res 104:933–942.
Sánchez V, Ferrán JL, Pereyra-Alfonso S, Scicolone G, Rapacioli M, Flores V. 2002. Developmental changes in the spatial pattern of mesencephalic trigeminal nucleus (Mes5) neuron populations in the developing chick optic tectum. J Comp Neurol 448:337–348.

Sanes DH, Reh TA, Harris WA. 2006. Genesis and migration. In: Menzel J, editor. Development of the Nervous System. Amsterdam, NL: Elsevier. pp 57–85.

Scicolone G, Pereyra-Alfonso S, Brusco A, Pecci Saavedra J, Flores V. 1995. Development of the laminated pattern of the chick embryo tectum opticum. Int J Dev Neurosci 13:845–858.

Seo JH, Chang JH, Song SH, Lee HN, Jeon GS, Kim DW, Chung CK, Cho SS. 2008. Spatiotemporal gradient of astrocyte development in the chick optic tectum: Evidence for multiple origins and migratory paths of astrocytes. Neurochem Res 33:1346–1355.

Sestan N, Artavanis-Tsakonas S, Rakic P. 1999. Contact-dependent inhibition of cortical neurite growth mediated by notch signaling. Science 286:741–746.

Streeter GL. 1948. Developmental horizons in human embryos: Description of age groups XV, XVI, XVII, and XVIII. Contrib Embryol 32:13–203.

Striedter GF, Beydler S. 1997. Distribution of radial glia in the developing telencephalon of chicks. J Comp Neurol 387:399–420.

Thanos S, Bonhoeffer F. 1987. Axonal arborization in the developing chick retinotectal system. J Comp Neurol 261:155–164.

Thanos S, Mey J. 2001. Development of the visual system of the chick II. Mechanisms of axonal guidance. Brain Res Brain Res Rev 35:205–245.

Trainor PA. 2005. Specification of neural crest cell formation and migration in mouse embryos. Semin Cell Dev Biol 16:683–693.

van den Berg G, Abu-Issa R, de Boer BA, Hutson MR, de Boer PA, Soufan AT, Ruijter JM, Kirby ML, van den Hoff MJ, Moorman AF. 2009. A caudal proliferating growth center contributes to both poles of the forming heart tube. Circ Res 104:179–188.

Whitford KL, Dijkhuizen P, Polleux F, Ghosh A. 2002. Molecular control of cortical dendrite development. Annu Rev Neurosci 25:127–149.

Wu CC, Russell RM, Karten HJ. 2000. Ontogeny of the tectorotundal pathway in chicks (*Gallus gallus*): Birthdating and pathway tracing study. J Comp Neurol 417:115–32.

Yamagata M, Weiner JA, Dulac C, Roth KA and Sanes JR. 2006. Labeled lines in the retinotectal system: Markers for retinorecipient sublaminae and the retinal ganglion cell subsets that innervate them. Mol Cell Neurosci 33:296–310.

Yasuda Y, Fujita S. 2003. Distribution of MAP1A, MAP1B, and MAP2A&B during layer formation in the optic tectum of developing chick embryos. Cell Tissue Res 314:315–324.